Erythromycin derivatives inhibit HIV-1 replication in macrophages through modulation of MAPK activity to induce small isoforms of C/EBPβ

Iwao Komuro*†, Toshiaki Sunazuka‡, Kiyoko S. Akagawa*‡, Yasuko Yokota*, Aikichi Iwamoto†, and Satoshi Ōmura‡§

*Department of Immunology, National Institute of Infectious Diseases, 1-23-1 Toyama, Shinjuku-ku, Tokyo 162-8640, Japan; †Division of Infectious Diseases, Advanced Clinical Research Center, Institute of Medical Science, University of Tokyo, 4-6-1 Shiroganedai, Minato-ku, Tokyo 108-8639, Japan; and ‡Kitasato Institute for Life Sciences, Kitasato University and the Kitasato Institute, 5-9-1 Shirokane, Minato-ku, Tokyo 108-8641, Japan

Contributed by Satoshi Ōmura, June 18, 2008 (sent for review January 11, 2008)

Macrophages (MΦs) are a major source of HIV-1 especially in patients with tuberculosis. There are MΦs that are permissive and those that restrict HIV-1. Regulation of hematopoietic cell kinase (Hck) activity and selective expression of CCAAT enhancer binding protein β (C/EBPβ) isoforms greatly contribute to determine distinct susceptibility of MΦs to HIV-1. Resistance is attributable to reduced expression of Hck and augmented expression of an inhibitory small isoform of C/EBPβ. Derivatives of erythromycin A (EMA) EM201 and EM703 inhibit the replication of HIV-1 in tissue MΦs, at posttranscriptional and translational levels. We demonstrate that EM201 and EM703 convert tissue MΦs from HIV-1 susceptible to HIV-1 resistant through down-regulation of Hck and induction of small isoforms of C/EBPβ. These drugs inhibit p38MAPK activation which is expressed only in susceptible tissue MΦs. Activated CD4+T cells stimulate the viral replication in HIV-1 resistant MΦs through down-regulation of small isoforms of C/EBPβ via activation of ERK1/2. EM201 and EM703 can inhibit the MAPK activation and inhibit the burst of viral replication produced when CD4+T cells and MΦs interact. These EM derivatives may be highly beneficial for repression of residual HIV-1 in the lymphoreticular system of HIV-1-infected patients and offer great promise for the creation of new anti-HIV drugs for the future treatment of AIDS patients.

AIDS | macrolides | Hck

At least 65 million people have been infected with HIV and AIDS has killed 25 million people since 1981. By 2007, worldwide, 39.5 million individuals were living with HIV, with 4.3 million new infections and 2.9 million deaths occurring in 2006 (http://data.unaids.org/pub/EpiReport/2006/02-Global_Summary_2006_EpiUpdate_eng.pdf). In developed countries, anti-HIV-1 therapy—highly active antiretroviral therapy (HAART)— potently inhibits HIV-1 replication, reduces viral antigenemia, and prolongs the survival of patients (1, 2). In contrast, patients in developing countries generally cannot use HAART therapy because of its high cost and the sheer number of patients. Furthermore, HAART therapy cannot remove HIV-1-infected latent memory T cells and monocytes (Mos)/macrophages (MΦs) in some lymphoreticular tissue, residual cells having the potential to become a viral resource capable of spreading new viral particles (3, 4). Therefore, the development of new drugs to improve and extend HAART therapy, particularly in countries in the developing world, is greatly and urgently needed.

Mos/MΦs are a major target of HIV-1 infection and serve as a reservoir for viral persistence and a chronic source of infectious virus *in vivo* (5). Most tissue MΦs are permissive to M-tropic virus entry and release a small number of virus particles in the asymptomatic carrier but they occasionally produce a large number of viral particles in the AIDS patients or HIV-1 patients with pulmonary tuberculosis (TB) or those whose conditions are complicated with opportunistic infection (3). TB markedly increases HIV-1 replication and mutation in the lung and is associated with an acceleration of AIDS (6, 7). The alveolar MΦ is the major cell type in which HIV-1 replication occurs during TB (8, 9). Thus MΦ is a key factor in the control of HIV-1 suffering.

We and others have previously demonstrated that expression of tyrosine kinase hematopoietic cell kinase (Hck) and relative amounts of a large isoform (37-kDa) to a small isoform (23-kDa) (L/S ratio) of transcription factor CCAAT enhancer binding protein β (C/EBPβ) play critical roles in M-tropic HIV-1 production in tissue MΦs (8, 10–13). We have also reported that modulation of the expression of Hck and the L/S ratio of C/EBPβ by treatment with antisense oligonucleotides can convert the phenotype of HIV-1 suceptibility in MΦs (10). These studies suggest that, not only anti-HIV-1 drugs that directly affect the virus (such as RT inhibitor or protease inhibitors), but also drugs that can convert the phenotype of tissue MΦs from "susceptible" to "resistant" by down-regulating the expression of Hck and enhancing the expression of small isoforms of C/EBPβ may be useful to help control HIV-1 replication in AIDS patients.

Macrolides with a 14-membered ring structure, such as erythromycin A (EMA), clarithromycin (CAM), or roxithromycin (RXM), are well known antibacterial drugs. Recently, these antibiotics have been shown to be efficacious against incurable chronic inflammatory airway disease, such as diffuse panbronchiolitis (DPB) (14, 15). This therapeutic efficacy is thought to be caused by either anti-inflammatory or immunomodulatory activity of the macrolide antibiotics, which can act on many cells, including epithelial cells, neutrophiles, monocytes/MΦs, and T cells (16–23). On the basis of this knowledge, we chemically modified EMA to obtain derivatives with both stronger capability for promoting monocyte-to-MΦ differentiation and no antibacterial activity. Among the derivatives, 8,9-anhydroerythromycin A 6,9-hemiketal (EM201), obtained by mild acid treatment of EMA, already known as an internal metabolite of EMA, showed a strong promotional effect on MΦ differentiation and possessed weak antimicrobial activity (24). Furthermore, the 12-membered pseudoerythromycin A (EM703) was both remarkably active and free of any antibacterial activity (25) and was known to exhibit a prophylactic effect on lung injury *in vivo* against a bleomycin-induced acute lung injury in the rat model, similar to EMA (26).

In this study, we show that both EM201 and EM703 are good lead candidates for drugs that can inhibit M-tropic HIV-1 replication in tissue MΦs by a new way of converting their phenotype from HIV-1-susceptible to HIV-1-resistant, through down-regulation of Hck and the induction of small isoforms of C/EBPβ via modulation of the activation of MAPKs.

Author contributions: T.S., K.S.A., and S.Ō. designed research; I.K., T.S., and K.S.A. performed research; T.S., Y.Y., and S.Ō. contributed new reagents/analytic tools; I.K., T.S., K.S.A., A.I., and S.Ō. analyzed data; and I.K., T.S., K.S.A., and S.Ō. wrote the paper.

The authors declare no conflict of interest.

§To whom correspondence should be addressed. E-mail: omuras@insti.kitasato-u.ac.jp.

This article contains supporting information online at www.pnas.org/cgi/content/full/0805504105/DCSupplemental.

© 2008 by The National Academy of Sciences of the USA

MICROBIOLOGY

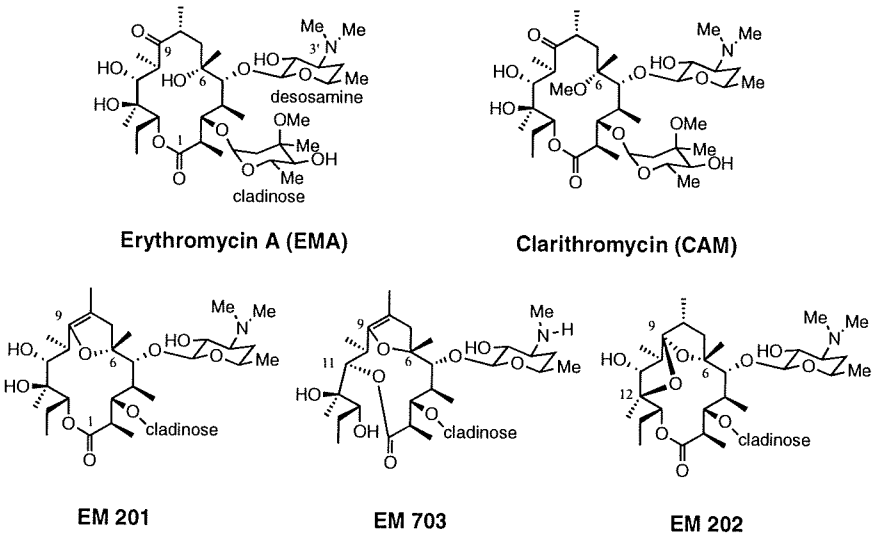

Fig. 1. Structure of EM derivatives.

Results

Effects of EM Derivatives on Viral Replication and Multinucleated Giant Cell Formation in M-Tropic HIV-1-Infected M-MΦs. We first examined whether EM derivatives (Fig. 1) have an ability to inhibit M-tropic HIV-1 replication in macrophage colony-stimulating factor (M-CSF)-induced monocyte-derived MΦs (M-MΦs), which express a high level of Hck and a large isoform of C/EBPβ, are susceptible to M-tropic HIV-1 replication, and whether they form multinucleated giant cells (MGC) by cell-to-cell fusion at 4–7 d after infection (10, 27). EM201 and EM703 (30 μM) completely inhibited viral replication and MGC formation at 7 d after infection, while EMA, CAM, and EM202 did not (Fig. 2*A*). PCR using a primer pair designed from the HIV-1 LTR region of HIV-1_{BaL} DNA at 2 d after infection showed that the DNA replication at first replicon was observed at similar levels in all of the M-MΦs. At 7 d after infection, however, the levels of viral DNA in M-MΦs treated with EMA, EM202, or DMSO (solvent) alone increased, whereas those in M-MΦs treated with EM201and EM703 remained low, at levels similar to those observed at 2 d after infection (Fig. 2*A*).

EM201 and EM703 (30 μM) persistently inhibited viral replication at 14 d (Fig. 2*B*), and inhibition was observed even at 21 d after infection (data not shown). EM201 and EM703 strongly inhibited HIV-1_{BaL} replication, even at 3 μM, and p24 levels were ~4% of those in cells treated with DMSO alone at 14 d after infection (Fig. 2*C*). EMA and EM202 induced inhibition of viral replication at higher concentration (>300 μM). However, the reduction curves in cells were similar to those in DMSO-treated cells (Fig. 2*C*), indicating the effects are mainly because of DMSO toxicity. In contrast, CAM partially but significantly inhibited HIV-1_{Bal} replication at 10–30 μM at 10 and 14 d after infection (Figs. 2 *B* and *C*), and it is impossible to deny that CAM itself can inhibit HIV-1 replication.

EM201 and EM703 Modulate the Expression of Hck and C/EBPβ Proteins in HIV-1_{BaL} Infected M-MΦs. To examine the possibility that EM201 and EM703 inhibit HIV-1 replication in M-MΦs via modulation of the expression of Hck and C/EBPβ, expression of these proteins in HIV-1 infected M-MΦs treated with 30 μM EM derivatives was examined by immunoblots at 2 d after infection. The levels of Hck protein in M-MΦs treated with EM201 and EM703 strongly decreased to one-seventh and one-ninth of that in M-MΦs treated with DMSO alone, respectively (Fig. 3*A*). Conversely, the small isoform of C/EBPβ protein was strongly induced in M-MΦs treated with EM201 and EM703, the levels increasing to 25- to 40-fold of that in M-MΦs treated with DMSO alone, with the L/S ratio of C/EBPβ markedly decreasing from 12.6 to 0.3 and 0.5, respectively (Fig. 3*A*).

EMA and EM202 did not affect the expression of Hck and C/EBPβ and consequently did not inhibit viral replication (Fig. 3*A*). Similarly CAM, which did not show inhibitory activity during the early phase of infection, did not significantly affect expression of either Hck or C/EBPβ at 2 d after infection.

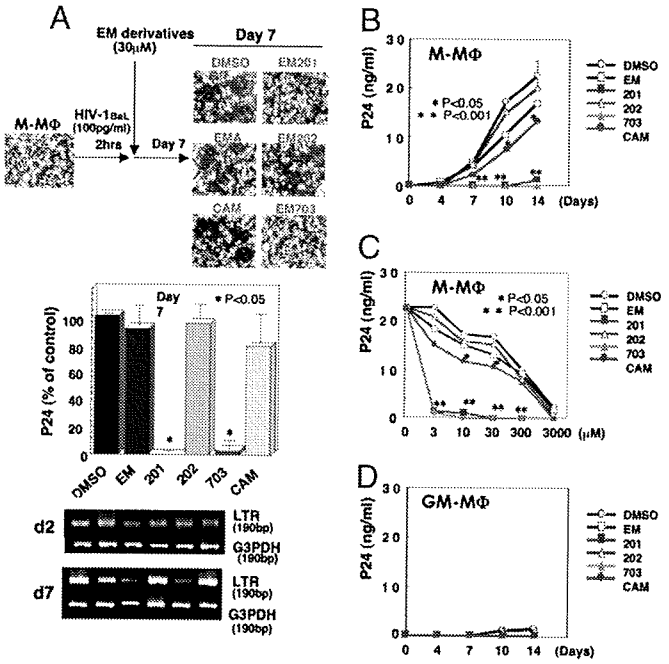

Fig. 2. Screening of EM derivatives that show an inhibitory effect on HIV-1_{BaL} replication in M-MΦs. (*A*) Effects of 30 μM of EMA (EM), CAM, EM201 (201), EM202 (202), and EM703 (703) on viral replication and MGC formation (Magnification, ×100) at 7 d after infection. The data of viral production were shown as the percentage of p24 antigen in control (DMSO alone) M-MΦs. The levels of viral DNA were assayed at 2 and 7 d after infection. (*B*) Kinetics of viral production in HIV-1 infected M-MΦs treated with 30 μM of EM derivatives. (*C*) Dose-response effects of EM derivatives on HIV-1 replication in M-MΦs at 14 d after infection. (*D*) EM derivatives (30 μM) do not change the resistant phenotype against HIV-1 infection in GM-MΦs. The data shown are representative one of five independent experiments.

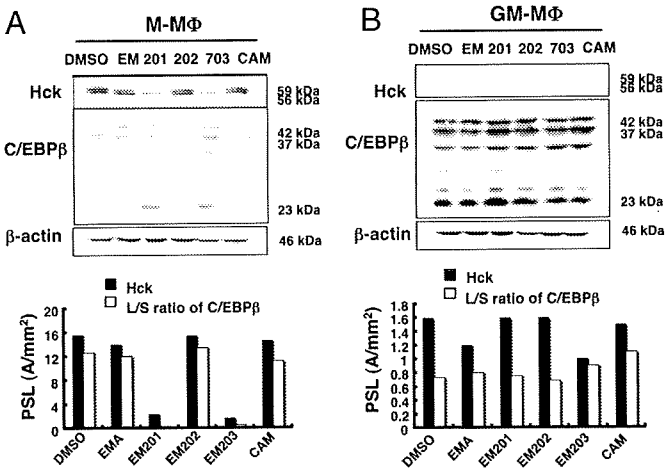

Fig. 3. Effects of EM derivatives on the expression of Hck and C/EBPβ in HIV-1_{BaL}-infected M-MΦs and GM-MΦs. Immunoblots of Hck and C/EBPβ in M-MΦs (*A*) and GM-MΦs (*B*) at 2 d after infection. EMA (EM), EM201 (201), EM202 (202), EM703 (703), and CAM were added at 30 μM. The relative amounts of Hck and C/EBPβ were measured using National Institutes of Health image software (PSL; photo stimulating luminescence, A/mm²). The relative amounts of the large band to the small band (L/S ratio) of C/EBPβ were calculated using PSL values of 37 kDa and 23 kDa of C/EBPβ isoforms and are shown at the bottom of each figure. The data shown are representative of one of three independent experiments.

EM201 and EM703 Change Neither the Expression of Hck and C/EBPβ Proteins Nor the Resistant Phenotype Against HIV-1 Infection in GM-MΦs. Granulocyte-macrophage CSF (GM-CSF)-induced monocyte-derived MΦ (GM-MΦ) is HIV-1 resistant and does not stimulate the replication of M-tropic HIV-1and MGC formation. This is because GM-MΦs express a high level of short isoforms of C/EBPβ and a low level of Hck, and HIV-1 infection drastically increases the expression of a short isoform of C/EBPβ but decreases that of Hck (10). We examined the effects of EM derivatives on viral replication and the expression of Hck and C/EBPβ in HIV-1_{BaL}-infected GM-MΦs. Even at 14 d after infection, we found that GM-MΦs treated with various kinds of EM derivatives (including EM201 and EM703) did not stimulate viral replication (Fig. 2*D*) or MGC formation (data not shown). Consistent with the lack of change in HIV-1 resistant phenotype, all of the EM derivatives did not affect the expression of Hck and C/EBPβ protein in GM-MΦs (Fig. 3*B*).

p38MAPK Inhibitor, but Not ERK1/2 Inhibitor, Inhibits Viral Replication in M-Tropic HIV-1 Infected M-MΦs via Reduced Expression of Hck and Increased Expression of a Small Isoform of C/EBPβ. Previous reports have shown that the replication of M-tropic HIV-1 in tissue MΦs requires the activation of p38MAPK (28) and that ERK1/2 mediates the activation of C/EBPβ (29, 30). We consequently examined the activation of MAPKs in HIV-1 susceptible M-MΦs and HIV-1 resistant GM-MΦs. Expressions of total and phosphorylated forms of p38MAPK in M-MΦs were higher than those in GM-MΦs before HIV-1_{BaL} infection (Fig. 4*A*). After infection, the phosphorylated form was augmented in M-MΦs but not in GM-MΦs (Fig. 4*A*). In contrast to p38MAPK, the expressions of total and phosphorylated forms of ERK1/2 in M-MΦs were lower than those in GM-MΦs before infection, but the expression was unchanged in both MΦs after infection (Fig. 4*A*). Consistent with the augumented activation of p38MAPK in M-MΦs, addition of p38MAPK inhibitor SB203580 (at 10 μM) completely suppressed viral replication and MGC formation in HIV-1_{BaL}-infected M-MΦs (Fig. 4*B*).

We subsequently investigated whether the inhibitory activity of SB203580 on viral replication in HIV-1_{BaL}-infected M-MΦs is mediated through modulation of the expression of Hck and C/EBPβ protein. SB203580 not only inhibited the phosphorylation of p38MAPK but also reduced the expression of Hck and increased the expression of the small isoform of C/EBPβ to mimic the inhibitory effect on viral replication (Fig. 4 *C–E*). Conversely, the ERK1/2 inhibitor PD98059 affected neither viral replication nor the expression of Hck and C/EBPβ protein (Fig. 4 *B–E*).

EM201 and EM703 Inhibit Viral Replication in M-Tropic HIV-1 Infected M-MΦs via Inhibition of p38MAPK Activation. The above results suggest that EM201 and EM703 inhibit M-tropic HIV-1 replication

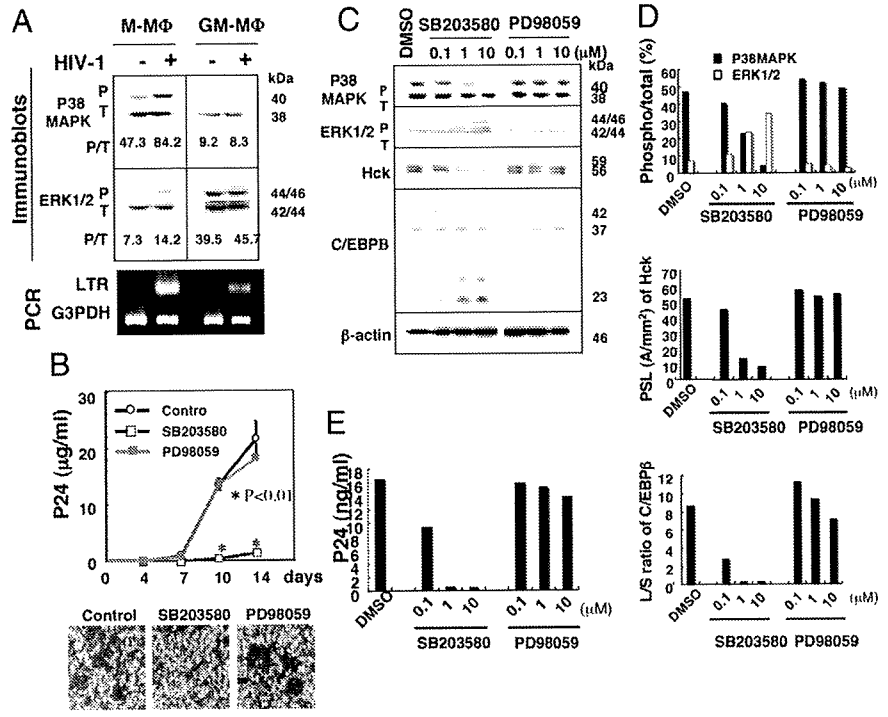

Fig. 4. Effects of p38 MAPK inhibitor and ERK1/2 inhibitor on viral replication and expression of Hck and C/EBPβ in HIV-1_{BaL}infected M-MΦs. (*A*) Immunoblot analysis of total and phosphorylated forms of p38MAPK and ERK1/2 in M-MΦs and GM-MΦs before and 2 d after infection. (*B*) Kinetic analysis of viral replication and morphology in HIV-1_{BaL}-infected M-MΦs treated with 10 μM of SB203580 or PD98059. (*C*) Immunoblot analysis of Hck and C/EBPβ in HIV-1_{BaL}-infected M-MΦs treated with various concentrations of SB203580 or PD98059 at 2 d after infection. (*D*) The relative amounts of Hck and L/S ratio of C/EBPβ in the cells or the phosphorylated protein *P* to the total protein *T* (P/T ratio) of p38 MAPK and ERK1/2 in immunoblot analysis shown in *c* calculated as described in Fig. 3. (*E*) Viral production in HIV-1_{BaL}-infected M-MΦs treated with various concentrations of SB203580 or PD98059. The data shown are representative of one of three independent experiments.

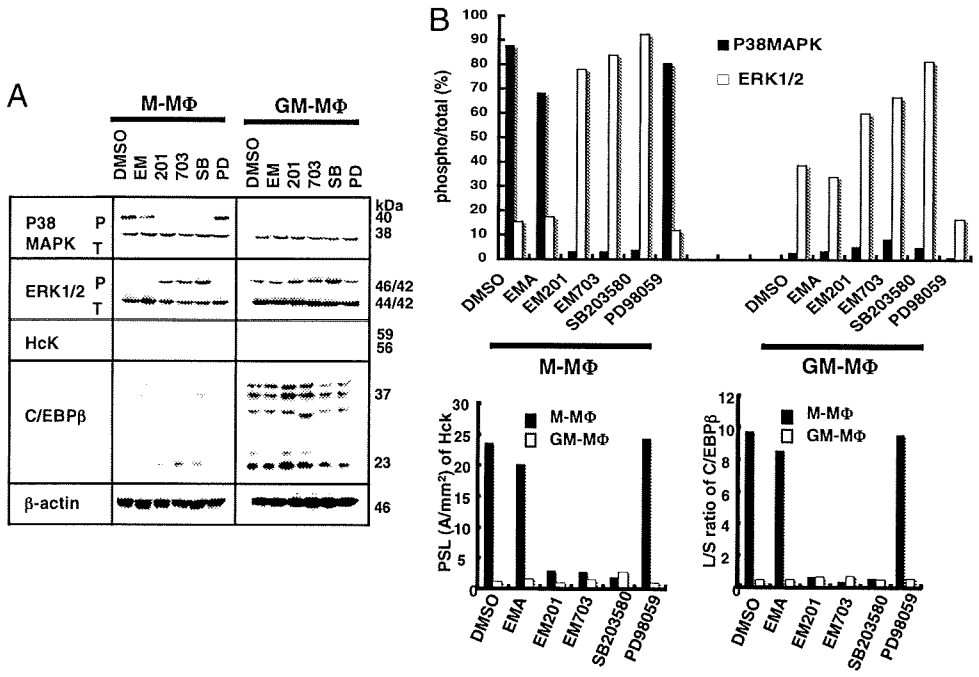

Fig. 5. Effects of EM derivatives on the phosphorylation of p38 MAPK and ERK1/2 in M-MΦs and GM-MΦs. (*A*) Immunoblot analysis of Hck and C/EBPβ, and the phosphorylation of p38 MAPK and ERK1/2 in M-MΦs and GM-MΦs treated with 30 μM of EMA (EM), EM201 (201), EM703 (703), 10 μM of SB203580 (SB), or PD98059 (PD), and DMSO alone at 2 d after HIV-1 infection. (*B*) The relative amounts of Hck and L/S ratio of C/EBPβ or P/T ratio of p38 MAPK and ERK1/2 in immunoblot analysis shown in *a* are calculated as described in Fig. 3. The data shown are representative of one of three independent experiments.

via inhibition of p38MAPK activation. To help confirm this hypothesis, we examined the effect of EM201 or EM703 (30 μM) on the phosphorylation of p38MAPK and ERK1/2 in M-MΦs by immunoblot. EM201 and EM703, but not EMA, reduced phosphorylation of p38MAPK but enhanced the phosphorylation of ERK1/2 in HIV-1-infected M-MΦs at 2 d after treatment (Fig. 5).

As described above, EM201 and EM703 did not affect the HIV-1-resistant phenotype of GM-MΦs (Figs. 2*D* and 3*B*). Consistent with the results, none of the EM derivatives significantly affected the phosphorylation pattern of p38MAPK and ERK1/2 in HIV-1-infected GM-MΦs (Fig. 5).

Activated CD4⁺T Cells Stimulate Viral Replication in M-Tropic HIV-1 Infected GM-MΦs via Down-Regulation of a Small Isoform of C/EBPβ. Recently, Hosino *et al.* (9) reported a phenotypical change of human alveolar MΦs (A-MΦs) from resistant to susceptible for HIV-1 replication caused by the addition of activated lymphocytes. The change was brought about by decreased expression of a small isoform of C/EBPβ (9). In line with this report, the addition of activated CD4⁺T cells to HIV-1_{BaL}-infected GM-MΦs stimulated marked viral replication (Fig. 6*A*), with MGC formation and clusters of GM-MΦs with CD4⁺ T cells (data not shown) at 10–14 d after infection. The amounts of viral DNA in the GM-MΦs increased at 2–7 d after infection (Fig. 6*B*). In GM-MΦs stimulated with activated CD4⁺ T cells, expression of the small isoform of C/EBPβ protein significantly decreased whereas the L/S ratio of C/EBPβ increased (from 0.57 to 3.6) at 2 d after infection (Fig. 6 *C* and *D*). Expression of Hck in the GM-MΦs, however, did not change significantly, even after stimulation with activated T cells and was very low compared with that in M-MΦs (Fig. 6 *C* and *D*).

Activated CD4⁺T Cells Down-Regulate the Small Isoform of C/EBPβ in M-Tropic HIV-1-Infected GM-MΦs via Augmentation of ERK1/2 Phosphorylation. As described above, activation of p38MAPK but not ERK1/2 is critical for HIV-1 replication in M-MΦs. However, the p38MAPK inhibitor, SB203580, did not inhibit viral replication in GM-MΦs stimulated with activated CD4⁺T cells (Fig. 6*A*). Instead, the ERK1/2 inhibitor PD98059 completely inhibited viral replication (Fig. 6*A*) and suppressed the level of viral DNA to that observed in the culture of GM-MΦs alone in which viral replication was absent (Fig. 6*B*). Upon examination of the phosphorylation of p38MAPK and ERK1/2 in HIV-1_{BaL}-infected GM-MΦs stimulated with activated CD4⁺ T cells, the phosphorylation ratio of ERK1/2 but not of p38MAPK significantly increased in GM-MΦs stimulated with activated CD4⁺ T cells, compared with that in GM-MΦs alone. Addition of PD98059 not only inhibited the phosphorylation of ERK1/2 but also increased expression of the small isoform of C/EBPβ, while markedly decreasing the L/S ratio of C/EBPβ from 3.6 to 0.82 (Fig. 6 *C* and *D*). The addition of SB203580 did not affect the expression of C/EBPβ. The expression of Hck was unaffected by treatment with either of the two inhibitors (Fig. 6 *C* and *D*).

EM201 and EM703 Inhibit M-Tropic HIV-1 Replication in GM-MΦs Stimulated with Activated CD4⁺ T Cells via Inhibition of the Activation of ERK1/2 and Augmentation of the Expression of the Small Isoform of C/EBPβ. In examining whether EM201 and EM703 can inhibit viral replication in M-tropic HIV-1-infected GM-MΦs stimulated with activated CD4⁺T cells, addition of EM201 and EM703 (30 μM) completely inhibited viral replication (Fig. 6*A*) and MGC formation (data not shown). The levels of HIV-1 DNA observed were very low, the same as those seen in the culture of GM-MΦs alone (Fig. 6*B*).

We subsequently examined the effects of EM201 and EM703 on the expression of Hck and C/EBPβ and on the phosphorylation of p38MAPK and ERK1/2 in HIV-1_{BaL}-infected GM-MΦs stimulated with activated CD4⁺ T cells at 2 d after infection by immunoblot. Treatment with EM201 and EM703 did not change the levels of Hck protein, but increased levels of the small isoform of C/EBPβ protein and the L/S ratio of C/EBPβ decreased from 3.6 to 0.45 (EM201) and 0.44 (EM703) (Fig. 6 *C* and *D*). The phosphorylation level of ERK1/2 decreased following treatment with EM201 and EM703, but that of p38MAPK remained unchanged (Fig. 6 *C* and *E*).

Discussion

In this study, we demonstrated that two EMA derivatives, EM201and EM703, can inhibit the replication of M-tropic HIV-1 in tissue MΦs at the posttranscriptional and translational levels, but do not affect viral entry and first DNA replicon. The inhibition is

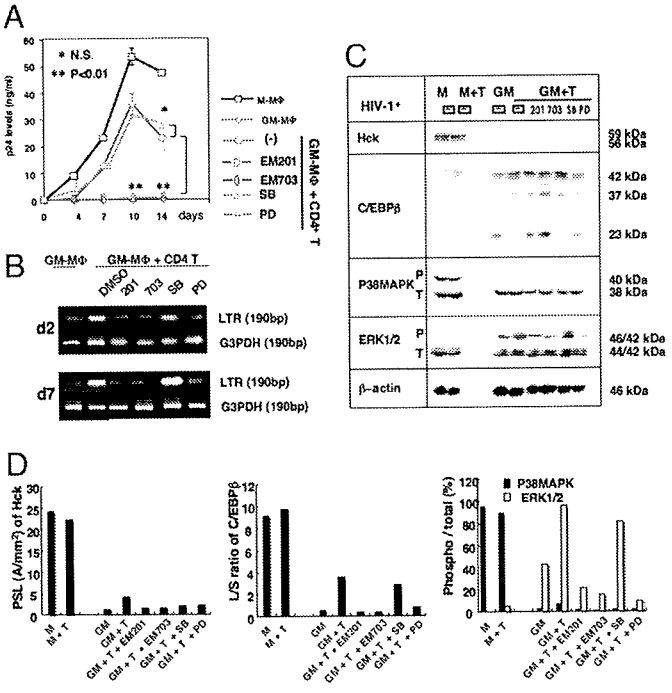

Fig. 6. Augmentation of M-tropic HIV-1 production in GM-MΦs stimulated with $CD4^+$ T cells, and the suppressive effects of EM201 and EM703 on viral replication through the induction of small isoforms of C/EBPβ via inhibition of phosphorylation of ERK1/2. M-MΦs and GM-MΦs were infected with $HIV\text{-}1_{BaL}$. Part of HIV-1-infected GM-MΦs were stimulated with activated $CD4^+$ T cells and incubated with or without 30 μM of EMA (EM), EM201 (201), or EM703 (703), 10 μM of SB203580 (SB), or PD98059 (PD), and DMSO alone. (*A*) Kinetic analysis of HIV-1 replication. (*B*) Levels of viral DNA at 2 and 7 d after infection. (*C*) Immunoblot analysis of Hck, C/EBPβ, and phosphorylation of p38 MAPK and ERK1/2 at 2 d after infection. (*D*) The relative amounts of Hck and L/S ratio of C/EBPβ or P/T ratio of p38 MAPK and ERK1/2 in immunoblot analysis shown in c calculated as described in Fig. 3. (*M*) M-MΦ; GM, GM-MΦ; T, T cells; 201, EM201; 703, EM703; SB, SB203580; and PD, PD98059. The data shown are representative of one of three independent experiments.

caused by a new means of converting the phenotype of tissue MΦs, from HIV-1 susceptible to HIV-1 resistant, via down-regulation of Hck and induction of the small isoform of C/EBPβ through modulation of the activation of MAPKs. Consistent with the previous report (9), we showed that HIV-1-resistant GM-MΦs, require stimulation with activated $CD4^+$T cells to produce vigorous virus production. This is mediated by down-regulation of the expression of the small isoform of C/EBPβ. Both EM201 and EM703 potently inhibit viral replication, not only in M-MΦs but also in GM-MΦs stimulated with activated $CD4^+$T cells via inhibiting the down-regulation of the expression of the small isoform of C/EBPβ.

Both EM201 and EM703 change the phenotype only of HIV-1-susceptible MΦs. They do not affect the phenotype of HIV-1-resistant GM-MΦs. HIV-1 susceptibility and the expression of Hck and C/EBPβ proteins in A-MΦs from normal healthy volunteers are the same as those in GM-MΦs (8, 10). Therefore EM201 and EM703 do not change the resistant phenotype of A-MΦs. This would be beneficial for healthy A-MΦs in the HIV-1 carrier, by maintaining resistance against HIV-1 replication.

In the present study, we demonstrated that activation of p38MAPK and ERK1/2 play a critical role in HIV-1 production via down-regulation of the small isoform of C/EBPβ in HIV-1-infected-M-MΦs and -GM-MΦs stimulated with activated $CD4^+$T cells, respectively. This study shows that different MAPKs play crucial roles in HIV-1 production in different types of tissue MΦs. P38MAPK activation in HIV-1-infected M-MΦs link to the augmented expression of Hck and the maintenance of the low level of the small isoform of C/EBPβ. We previously reported that reduced expression of Hck in M-MΦs with antisense oligonucleotide for Hck stimulates the induction of the short isoform of C/EBPβ and inhibits the viral replication (10). Our present results, taken together with the previous study, show the unique evidence that the p38MAPK signal cascade is upstream of Hck expression and is linked to down-regulation of the small isoform of C/EBPβ in HIV-1-susceptible M-MΦs. However, ERK1/2-mediated down-regulation of the small isoform of C/EBPβ in HIV-1-infected GM-MΦs stimulated with activated $CD4^+$T cells does not link to Hck expression.

Interestingly, EM201 and EM703, in contrast to existing MAPK inhibitors, can inhibit viral replication via prevention of the activation of respective MAPKs in both HIV-1-infected-M-MΦs and -GM-MΦs stimulated with activated T cells, where different MAPKs play a critical role for viral replication. Such a novel and unique suppressive mechanism of EM201 and EM703 on HIV-1 replication in tissue MΦs may be useful for the future treatment of AIDS patient.

The anti-HIV-1 activity of EM201 and EM703 does not relate to their antibiotic activity, because they have only weak (EM201) or completely lack (EM703) such antibiotic activity (24, 25). At present, we do not know what kind of structure activity relationships exist in EM201 and EM703. Recently, calmodulin- and calmodulin-dependent protein kinase-II (CaMK-II)-dependent activation of p38MAPK has been reported in HIV accessory protein, Tat-induced IL-10 expression in normal human monocytes (31). EM201 and EM703 are known to act as inhibitors of intracellular Ca^{2+} level and Ca^{2+} oscillation (21, 32, 33). These characteristics may contribute to the novel anti-HIV-1 mechanism of EM201 and EM703.

Macrolides, such as EMA and CAM, are known to be specifically accumulated into tissue MΦs and stay stable at high levels for long periods because of a low rate of breakdown and excretion (34). EM201 and EM703 potently inhibit HIV-1 replication in MΦs at low levels, such as 30 μM, that correspond to the concentration of EMA or CAM in MΦs after oral intake of EMA, 400 mg or CAM 200 mg/day (usual doses are 1600 mg and 400 mg/day, respectively). Furthermore, inhibition of viral replication can be observed at lower concentrations, such as 3 μM, which is sustained for 2–14 days after infection. These findings offer advantages with respect to drug specificity and reduction of drug toxicity. In addition, these new macrolides are derived from EMA (24, 25) and would be very inexpensive. Thus, these substances offer great potential for the creation of new anti-HIV-1 drugs for the future treatment of AIDS patients.

Materials and Methods

Erythromycin Derivatives. EMA was purchased from Sigma-Aldrich. CAM was supplied by Taisho Pharmaceutical. EM201, EM202, and EM703 were prepared as described previously (24, 25).

Preparation and Culture of MΦs. Monocytes (Mos) and Mo-derived Mp were prepared as described previously (10, 35). M-CSF-induced monocyte-derived MΦs and GM-CSF-induced monocyte-derived MΦs were called M-MΦs and GM-MΦs, respectively. [see supporting information (SI) *Materials and Methods* for a detailed description].

HIV-1 Strain and Infection. M-tropic HIV-1 strain, $HIV\text{-}1_{BaL}$, was collected from culture supernatant of the HIV-1 strain-infected M-MΦs as a viral resource. Mo-derived MΦs were incubated for 2 h at 37°C with 100 pg/ml p24 antigen of DNase-treated viral supernatant (p24, the 50% tissue culture infective dose ($TCID_{50}$) and multiplicity of infection (MOI) are 50 ng/ml, ~3,000 and 0.05, respectively) and then cultured in RPMI MEDIUM 1640 containing 10% FCS and CSF. If necessary, the viral inoculum was pretreated with 100 μM AZT for 2 h at 4°C (5). Fresh culture medium containing CSF was added every 3–4 d (20% of the volume). Heat-inactivated virus (1 h, 56°C) was used as negative control. Viral production was assayed by sequential measurement of p24 antigen in superna-

tants by an ELISA using a combination of two antibodies; anti-*gag*-p24 monoclonal antibody (Nu24) and peroxidase-labeled 10B5 (36), or the RETRO-TEK HIV-1 p24 antigen ELISA kit for high-affinity detection of low levels of p24 antigen (ZeptoMetrix, Buffalo, New York).

Coculture of HIV-1 Infected GM-MΦs with the Activated CD4$^+$T Cells. CD4$^+$ T cells were positively isolated from CD14$^-$ PBMCs using a MACS with anti-CD4 mAb coated microbeads. The selected population was >93% positive for CD3 and CD4. Activated CD4$^+$ T cells were prepared by stimulation with PHA and cultured with IL-2 (30 unit/ml) (Genzyme). GM-MΦs were incubated for 2 h at 37°C with 100 pg/ml p24 antigen of DNase-treated viral supernatant, washed twice, and then cocultured with the activated CD4$^+$ T cells in the presence of IL-2.

Detection of HIV-1 DNA by Nested PCR. Detection of HIV-1 DNA by nested PCR was performed as described previoiusly (10). HIV LTR and *gag* primers were JAM 62 and JAM 65. For the nested PCR, JAM 63 and JAM 64 were used as internal primers (36). (see *SI Materials and Methods* for a detailed description).

Immunblot Analysis. Immunoblot analysis was performed as described in ref. 10. Antibodies against the following proteins were used: rabbit polyclonal antibody against Hck (N-30), C/EBPβ (C-19) (Santa Cruz Biotechnology), phospho-specific (Tyr 182) p38 mitogen-activated protein kinase (P38MAPK) (no. 9211), p38 MAPK (no. 9212), phospho-specific (Tyr 204) phosphorylated extracellular signal-regulated kinases (ERK)1/2 (no. 9101), ERK1/2 antibody (no. 9102) (New England BioLabs), or normal rabbit IgG. Horseradish peroxidase-conjugated goat anti-rabbit IfG (sx-2030)(Santa Cruz Biotechnology) was used as secondary Ab. The blots were visualized with Amersham ECL Reagent on Hyper ECL-film (Amersham). (see *SI Materials and Methods* for a detailed description).

Statistical Analysis. Statistical analysis of the data were performed using Student's *t test*. *P*-values <0.01 were considered significant. The experiments shown are representatives of three to seven independent experiments.

ACKNOWLEDGMENTS. This work was supported in part by grants for Research on Health Sciences Focusing on Drug Innovation from the Japan Health Sciences Foundation and the Ministry of Health, Labor and Welfare of Japan.

1. Cavert W, *et al.* (1997) Kinetics of response in lymphoid tissues to antiretroviral therapy of HIV-1 infection. *Science* 276:960–964.
2. Perelson AS, *et al.* (1997) Decay characteristics of HIV-1-infected compartments during combination therapy. *Nature* 387:188–191.
3. Orenstein JM, Fox C, Wahl SM (1997) Macrophages as a source of HIV during opportunistic infections. *Science* 276:1857–1861.
4. Crowe SM, Sonza S (2000) HIV-1 can be recovered from a variety of cells including peripheral blood monocytes of patients receiving highly active antiretroviral therapy: A further obstacle to eradication. *J Leukoc Biol* 68:345–350.
5. Orenstein JM (2001) The macrophage in HIV infection. *Immunobiol* 204:598–602.
6. Nakata K, *et al.* (1997) Mycobacterium tuberculosis enhances human immunodeficiency virus-1 replication in the lung. *Am J Resp Crit Care Med* 155:996–1003.
7. Whalen C, *et al.* (1995) Accelerated course of human immunodeficiency virus infection after tuberculosis. *Am J Respir Crit Care Med* 151:129–135.
8. Honda Y, *et al.* (1998) Type I interferon induces inhibitory 16-kD CCAAT/enhancer binding protein (C/EBP)beta, repressing the HIV-1 long terminal repeat in macrophages: Pulmonary tuberculosis alters C/EBP expression, enhancing HIV-1 replication. *J Exp Med* 188:1255–1265.
9. Hoshino Y, *et al.* (2002) Maximal HIV-1 replication in alveolar macrophages during tuberculosis requires both lymphocyte contact and cytokines. *J Exp Med* 195:495–505.
10. Komuro I, Yokota Y, Yasuda S, Iwamoto A, Akagawa KS (2003) CSF-induced and HIV-1-mediated distinct regulation of Hck and C/EBPbeta represent a heterogeneous susceptibility of monocyte-derived macrophages to M-tropic HIV-1 infection. *J Exp Med* 198:443–453.
11. Henderson AJ, Calame KL (1997) CCAAT/enhancer binding protein (C/EBP) sites are required for HIV-1 replication in primary macrophages but not CD4(+) T cells. *Proc Natl Acad Sci USA* 94:8714–8719.
12. Weiden M, *et al.* (2000) Differentiation of monocytes to macrophages switches the mycobacterium tuberculosis effect on HIV-1 replication from stimulation to inhibition: Modulation of interferon response and CCAAT/enhancer binding protein beta expression Type I interferon induces inhibitory 16-kD CCAAT/enhancer binding protein (C/EBP)beta, repressing the HIV-1 long terminal repeat in macrophages: Pulmonary tuberculosis alters C/EBP expression, enhancing HIV-1 replication. *J Immunol* 165:2028–2039.
13. Hogan TH, Krebs FC, Wigdahl B (2002) Regulation of human immunodeficiency virus type 1 gene expression and pathogenesis by CCAAT/enhancer binding proteins in cells of the monocyte/macrophage lineage. *J Neurovirol* 8 Suppl 2:21–26.
14. Kudoh S, Uetake K, Hagiwara K (1987) Clinical effect of low dose long term erythromycin chemotherapy on diffuse panbronchiolitis. *Jap J Thorac Dis* 25:632–642.
15. Kadota J, *et al.* (1993) A mechanism of erythromycin treatment in patients with diffuse panbronchiolitis. *Am Rev Respir Dis* 147:153–159.
16. Sugawara E (1997) Effect of macrolide antibiotics on neutrophil function in human peripheral blood. *Kansenshogaku Zasshi* 71:329–336.
17. Sunazuka T, *et al.* (1999) Effects of erythromycin and its derivatives on Interleukin-8 release by human bronchial epithelial cell line BEAS-2B cells. *J Antibiot* 52:71–74.
18. Oohori M, *et al.* (2000) Effect of 14-membered ring macrolide compounds on rat leucocytes chemotaxis and the structure-activity relationships. *J Antibiot* 53:1219–1222.
19. Keicho N, Kudoh S, Yotsumoto H, Akagawa KS (1993) Erythromycin promotes monocytes to macrophage differentiation. *J Antibiot* 47:80–89.
20. Keicho N, Kudoh S, Yotsumoto H, Akagawa KS (1993) Antilymphocytic activity of erythromycin distinct from that of FK506 or cyclosporin A. *J Antibiot* 46:1406–1413.
21. Kudoh S, *et al.* (2002) Novel activity of erythromycin and its derivatives. *Macrolide Antibiotics, Chemistry, Biology, and Practice*, eds Omura S (Academic), 2nd Ed, pp 533–569.
22. Culic O, Erakovic V, Parnham MJ (2001) Anti-inflammatory effects of macrolide antibiotics. *Eur J Pharmacol* 429:209–229.
23. Labro MT (2001) Anti-inflammatory activity of macrolides: A new therapeutic potential? *J Antimicrob Chemother* 41(Suppl B):37–46.
24. Sunazuka T, *et al.* (2003) Effect of 14-membered macrolide compounds on monocyte to macrophage differentiation. *J Antibiot* 5:721–724.
25. Yoshida K, *et al.* (2005) Macrolides with promotive activity of monocyte to macrophage differentiation. *J Antibiot* 58:79–81.
26. Ying JL, *et al.* (2006) EM703 improves bleomycin-induced pulmonary fibrosis in mice by the inhibition of TGF-beta signaling in lung fibroblasts. *Respir Res* 7:16:1–13.
27. Matsuda S, *et al.* (1995) Suppression of HIV replication in human monocyte-derived macrophages induced by granulocyte/macrophage colony-stimulating factor. *AIDS Res Hum Retroviruses* 11:1031–1038.
28. Muthumani K, *et al.* (2004) Suppression of HIV-1 viral replication and cellular pathogenesis by a novel p38/JNK kinase inhibitor. *Aids* 18:739–748.
29. Nakajima T, *et al.* (1993) Phosphorylation at threonine-235 by a ras-dependent mitogen-activated protein kinase cascade is essential for transcription factor NF-IL6. *Proc Natl Acad Sci USA* 90:2207–2211.
30. Giltiay NV, Karakashian AA, Alimov AP, Ligthle S, Nikolova-Karakashian MN (2005) Ceramide- and ERK-dependent pathway for the activation of CCAAT/enhancer binding protein by interleukin-1beta in hepatocytes. *J Lipid Res* 46:2497–2505.
31. Gee K, Angel JB, Mishra S, Blahoianu MA, Kumar A (2007) IL-10 regulation by HIV-Tat in primary human monocytic cells: Involvement of calmodulin/calmodulin-dependent protein kinase-activated p38 MAPK and Sp-1 and CREB-1 transcription factors. *J Immunol* 178:798–807.
32. Sunazuka T, Omura S (2004) Creation of a new macrolide derivative, EM703. *Jpn J Antibiot* 57(Suppl A):114–116.
33. Hattori R, Shimizu T, Shimizu S, Majima Y (2004) Effect of EM703, a new macrolide derivative, on mucus secretion from the airway epithelial cells. *Jpn J Antibiot* 57(Suppl A):123–125.
34. Fietta A, Merlini C, Gialdroni GG (1997) Requirements for intracellular accumulation and release of clarithromycin and azithromycin by human phagocytes. *J chemotherapy* 9:23–31.
35. Akagawa KS (2002) Functional heterogeneity of colony-stimulating factor induced human monocyte-derived macrophages. *Int J Hematol* 76:27–34.
36. Tsunetsugu-Yokota Y, *et al.* (1995) Monocyte-derived cultured dendritic cells are susceptible to human immunodeficiency virus infection and transmit virus to resting T cells in the process of nominal antigen presentation. *J Virol* 69:4544–4547.

Biochemical and Biophysical Research Communications 377 (2008) 7–11

Contents lists available at ScienceDirect

Biochemical and Biophysical Research Communications

journal homepage: www.elsevier.com/locate/ybbrc

A recombinant replication-competent hepatitis C virus expressing Azami-Green, a bright green-emitting fluorescent protein, suitable for visualization of infected cells

Wei Hou [a], Chie Aoki [a,b], Lijuan Yu [a], Xianzi Wen [a], Yinhuan Xue [a], Bin Gao [a], Wenjun Liu [a], George Fu Gao [a], Aikichi Iwamoto [a,b,c], Yoshihiro Kitamura [a,b,*]

[a] China–Japan Joint Laboratory of Molecular Immunology and Molecular Microbiology, Institute of Microbiology, Chinese Academy of Sciences, No. A 3 Datun Road, Chaoyang District, Beijing 100101, China
[b] Research Center for Asian Infectious Diseases, The Institute of Medical Science, The University of Tokyo, 4-6-1 Shirokanedai, Minato-ku, Tokyo 108-8639, Japan
[c] Division of Infectious Diseases, Advanced Clinical Research Center, The Institute of Medical Science, The University of Tokyo, 4-6-1 Shirokanedai, Minato-ku, Tokyo 108-8639, Japan

ARTICLE INFO

Article history:
Received 30 July 2008
Available online 9 September 2008

Keywords:
Hepatitis C virus
JFH1
Azami-Green
Nonstructural protein 5A
Interferon

ABSTRACT

The hepatitis C virus (HCV) production system consists of transfecting the human hepatoma cell line Huh7 with genomic HCV RNA (JFH1). To monitor HCV replication by fluorescence microscopy, we constructed a recombinant HCV clone expressing Azami-Green (mAG), a bright green fluorescent protein, by inserting the mAG gene into the nonstructural protein 5A (NS5A) gene; the resultant clone was designated JFH1-hmAG. The Huh-7.5.1 (a subclone of Huh7) cells transfected with JFH1-hmAG RNA were found to produce cytoplasmic NS5A-mAG, as readily visualized by fluorescence microscopy, and infectious virus, as assayed with the culture supernatant, indicating that JFH1-hmAG is infectious and replication-competent. Furthermore, the replication of this virus was inhibited by interferon alpha in a dose-dependent manner. These results suggest that JFH1-hmAG is useful for studying HCV life cycle and the mechanism of interferon's anti-HCV action and for screening and testing new anti-HCV drugs.
© 2008 Elsevier Inc. All rights reserved.

Hepatitis C virus (HCV), a positive-strand RNA virus, which belongs to *Flaviviridae*, causes serious chronic hepatitis that results in cirrhosis and hepatocellular carcinoma. Recently, cell culture systems supporting HCV replication have been developed with the complementary DNA clones of the genotype 2a isolate JFH1 [1–7] and the genotype 1a isolate H77S [8]. These systems have been shown to greatly contribute to the studies of HCV biology and the development of novel antiviral strategies against HCV [9–24]. However, the procedures for quantitative analysis of HCV are considerably complicated, because the yield of HCV in cell cultures is fairly low. Moreover, observation of living infected cells has been impossible. For solving these problems, development of recombinant HCV carrying a reporter gene such as *Renilla* luciferase or red/green fluorescent protein gene has been attempted [25–27].

A green-emitting fluorescent protein, Azami-Green (AG, tetrameric) has been identified in a stony coral, *Azami-Sango* [28]. Its monomeric derivative (mAG) is stably brilliant independently of pH and thus suitable for labeling proteins or subcellular structures in mammalian cells [28]. Most importantly, as far as we know, mAG is the brightest among the monomeric forms of green-emitting fluorescent proteins; for example, it is approximately 1.23-fold brighter than EGFP from *Aequorea victoria* [28,29] (brightness is calculated as a product of molar extinction coefficient and fluorescence quantum yield). In this study, inserting an mAG gene with humanized codon usage (hmAG) into the nonstructural protein 5A (NS5A)-coding sequence, we generated a novel replication-competent HCV clone. The brightness of the mAG allowed us to visualize infected cells with high sensitivity and ease.

Materials and methods

HCV plasmid construction. The DNA fragment encoding a monomeric Azami-Green (mAG) with the *Xho*I sites (C'TCGAG) at both ends was obtained by PCR using phmAG1-MC1 (MBL, Tokyo, Japan) as a template, digested with *Xho*I, and inserted into the *Abs*I site (5′-CCTCGAGG-3′) of pJFH1 [1] (GenBank Accession No. AB047639). The integrity of the resulting plasmid, pJFH1-hmAG was verified by DNA sequencing (Fig. 1).

RNA synthesis. We followed previously developed methods [30]. In brief, we cut pJFH1-hmAG with *Xba*I and treated it with Mung

* Corresponding author. Address: China–Japan Joint Laboratory of Molecular Immunology and Molecular Microbiology, Institute of Microbiology, Chinese Academy of Sciences, No. A 3 Datun Road, Chaoyang District, Beijing 100101, China.
E-mail address: kitamura@im.ac.cn (Y. Kitamura).

0006-291X/$ - see front matter © 2008 Elsevier Inc. All rights reserved.
doi:10.1016/j.bbrc.2008.08.145

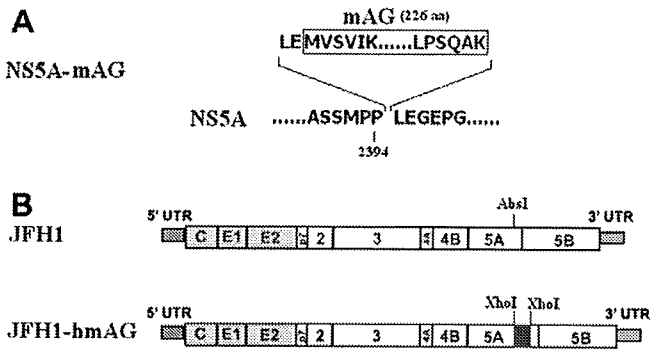

Fig. 1. HCV plasmids. (A) Sites and amino acid sequences of the mAG insertion in NS5A. (B) Schematic diagrams of JFH1 and its derivative JFH1-hmAG containing the hmAG gene within the NS5A gene.

Bean nuclease (New England Biolabs) to remove the 3′-protruding four nucleotides. With this DNA, we synthesized HCV RNA by using a MEGAscript™ T7 kit (Applied Biosystems/Ambion, TX). We treated the synthesized RNA with DNaseI (Promega, WI) at 37 °C for 15 min, and extracted it with acid phenol to remove remaining template DNA.

Cell cultures and transfection. Huh-7.5.1 cells [2], which are highly permissive to HCV RNA replication, were maintained in Dulbecco's modified Eagle's medium (DMEM) (Sigma-Aldrich, MO) supplemented with 10% fetal bovine serum (Invitrogen Corporation/Gibco, CA), 100 μg/mL of kanamycin (Sigma), and non-essential amino acids (Invitrogen Corporation/Gibco). The synthesized RNA of JFH1-hmAG was delivered to cells by electroporation or lipofection. We performed electroporation with a Gene Pulser II apparatus (Bio-Rad Laboratories, CA) as described [1], and lipofection with UniFECTOR reagent (B-Bridge International, Tokyo, Japan); a mixture of 6 μg of JFH1-hmAG RNA and 36 μl of UniFECTOR was subjected to 10^6 cells in a 100-mm culture dish.

Immunofluorescence analysis. Intracellular staining was performed as described [2]. In brief, a anti-Core mouse monoclonal antibody (IgG1, clone Hyb-K0811B, Cosmo Bio, Tokyo, Japan) was used at a dilution of 1:200 followed by incubation with a 1:400 dilution of Alexa Fluor 594-conjugated donkey anti-mouse antibody (Invitrogen Corporation/Molecular Probes, CA). Cell nuclei were stained with 4,6-diamidino-2-phenylindole (DAPI, Sigma-Aldrich). Images were acquired by using Biozero fluorescence microscopy (Keyence, Tokyo, Japan) or with a confocal microscope Leica TCS SP2 (Leica Microsystems GmbH, Wetzlar, Germany).

Infection. Huh-7.5.1 cells were seeded 24 h before infection at a density of 2×10^4 cells/well in a 8-well culture slide (BD BioCoat™, poly-D-lysine coated 8-well CultureSlide, BD, NJ). The cells were inoculated with the culture supernatant obtained from the cells transfected with JFH1-hmAG RNA for 3 h, washed three times with PBS, then cultured in 0.5 mL/well of the complete culture medium.

Reverse transcription (RT) PCR. RNA was extracted from cell culture supernatant with ISOGEN-LS (Nippon GENE, Tokyo, Japan) or from cells with ISOGEN (Nippon GENE). Complementary DNA was generated by a ReverTra Ace qPCR RT kit (Toyobo, Osaka, Japan) according to manufacturer's instructions. PCRs targeting the different regions along the JFH1-hmAG genome were performed. The primers for PCR were as follows: for the 5′-untranslated region (5′UTR), 5′-TCTGCGGAACCGGTGAGTAC-3′ and 5′-TCAGGCAGTACC ACAAGGCC-3′); for the nonstructural protein 3 (NS3) region, 5′-C TTTGACTCCGTGATCGACC-3′ and 5′-CCCTGTCTTCCTCTACCTG-3′; and for the NS5A-hmAG junction, 5′-CTGGCCATCAAGACCTTTG-3′ and 5′-GCTTGAAGTAGTCCTGGATG-3′.

Interferon inhibition. Huh-7.5.1 cells were incubated for 12 h with various concentrations of interferon alpha (IFNα, Universal Type I Interferon, PBL InterferonSource, NJ), then incubated with the culture supernatant containing JFH1-hmAG virus for 3 h, washed twice with PBS, and further incubated for 3 days. The copy numbers of intracellular HCV RNA were determined by quantitative RT-PCR (RT-qPCR). RT-qPCR with a LightCycler 2.0 Instrument (Roche) allowed us to determine relative copy numbers by normalization with that of GAPDH mRNA. The primers for RT-qPCR were as follows: for HCV, 5′-TCTGCGGAACCGGTGAGTA-3′ (sense) and 5′-TCAGGCAGTACCACAAGGC-3′ (antisense); and for GAPDH, 5′-G AAGGTGAAGGTCGGAGTC-3′ (sense) and 5′-GAAGATGGTGATGGG ATTTC-3′ (antisense), as described previously [2,31].

Results and discussion

Construction of pJFH1-hmAG and direct visualization of NS5A-mAG by fluorescent microscopy

We constructed a novel HCV clone (JFH1-hmAG) containing the hmAG sequence fused with NS5A at the amino acid 418 of NS5A (see Materials and methods for detail. Fig. 1). Three days after transfection of Huh-7.5.1 cells with JFH1-hmAG RNA, the green signal of the NS5A-mAG fluorescence was strong enough to be readily visualized in the cytoplasm as bright dots in a reticular pattern surrounding the nucleus by confocal microscopy (Fig. 2A). To further confirm viral protein production, we stained the cells with anti-Core antibody (Fig. 2B, upper right) and found the signal in a pattern similar to that of NS5A-mAG. Indeed, merging the NS5A-mAG and Core images (Fig. 2B, lower right), we observed partial colocalization of NS5A-mAG and Core, shown as yellow signals. Since the wild-type JFH1 has been reported to show the same colocalization pattern [25,32], JFH1-hmAG seems to inherit this property from the wild-type JFH1. Furthermore, RT-PCR with the RNA extracted from these transfected cells showed that the NS5A-hmAG junction in the JFH1-hmAG genome was stably retained (data not shown). Further studies seem necessary to determine the stability of NS5A-mAG over more extended passages indicator.

Inoculation of naïve Huh-7.5.1 cells with the supernatant of transfected cells

To test whether the reporter construct JFH1-hmAG can produce and release infectious virus particles, we inoculated naïve Huh-7.5.1 cells with the culture supernatant obtained from the transfected cells 30 days after transfection with JFH1-hmAG RNA. Two days after inoculation, NS5A-mAG signal was visualized in infected cells by fluorescence microscopy while not in uninfected cells (Fig. 2C). Immunostaining showed the same colocalization configuration of NS5A-mAG and Core proteins in inoculated cells (Fig. 2D) as in the transfected cells (Fig. 2B). Therefore, we considered that the new recombinant virus replicates in the same manner as the parental JFH1, even though NS5A was truncated by insertion of hmAG. Moreover, the RNA in cells and supernatants was considered to keep integrity without loss of the inserted mAG because all the RT-PCRs targeting the 5′UTR, NS3, and NS5A-hmAG junction regions yielded the products with predicted sizes (Fig. 3).

Taken altogether, we concluded that the JFH1-hmAG clone is infectious and replication-competent. In the transfected cells, JFH1-hmAG RNA produced NS5A-mAG/Core proteins, replicated, and released HCV particles that were infectious to Huh-7.5.1 cells. Though the culture supernatants of transfected cells at different time points were capable of infecting and re-infecting Huh-7.5.1 cells (data not shown), further studies seem necessary to

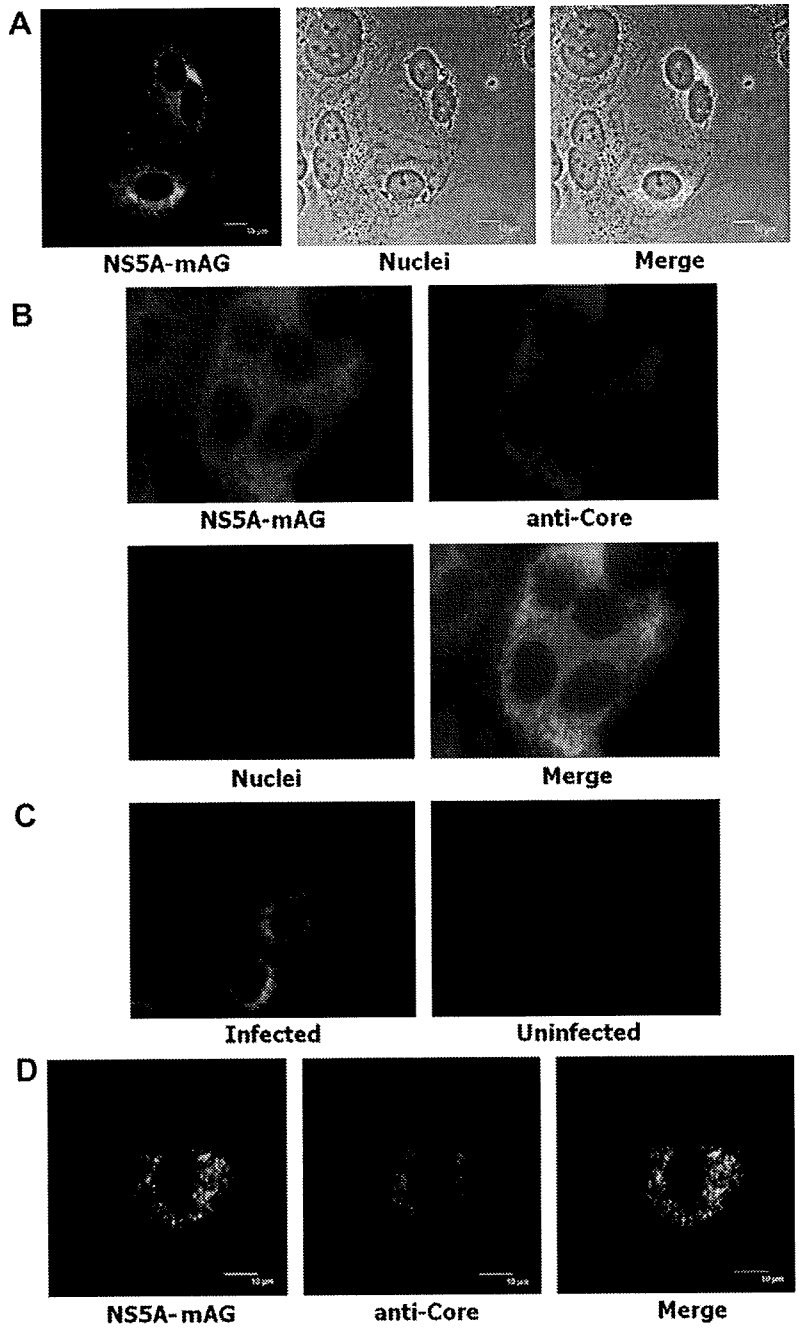

Fig. 2. Cell Images by fluorescence microscopy. (A) Huh-7.5.1 cells were analyzed by confocal microscopy 3 days after transfection with JFH1-hmAG RNA. The mAG emitted green signals. (B) Subcellular localization of NS5A-mAG and Core proteins in transfected cells. Huh-7.5.1 cells transfected with JFH1-hmAG RNA were grown in a 8-well chamber for 3 days. Cells were stained with monoclonal anti-Core mouse antibody and Alexa Fluor 594-conjugated donkey anti-mouse antibody. The localization patterns of NS5A-mAG and Core were shown in green and red, respectively. The merged images were also shown. Nuclei were stained with DAPI (blue). (C) NS5A-mAG was directly visualized in Huh-7.5.1 cells by fluorescence microscopy after inoculation with the culture supernatant obtained from the transfected cells 30 days after RNA transfection. (D) Subcellular localization of NS5A-mAG and Core protein in infected cells. NS5A-mAG and Core proteins were visualized 2 days after inoculation as described in (B).

determine the infectivity and integrity of JFH1-hmAG virus for a longer period, since genetic mutations frequently appeared in an persistent HCV infection in vitro [33].

Inhibition of JFH1-hmAG infection by interferon (IFN)

The current standard therapy to chronic hepatitis C includes IFN [34]. JFH1 replication has been found to be sensitive to IFN [2]. To test IFN-sensitivity of JFH1-hmAG, we examined the viral infection in the presence of IFNα. Huh-7.5.1 cells were pretreated for 12 h with IFNα and then were incubated with the culture supernatant containing JFH1-hmAG virus. Three days after infection, the levels of intracellular HCV RNA were determined by RT-qPCR (Fig. 4). IFNα pretreatment inhibited JFH1-hmAG RNA accumulation in a dose-dependent manner (Fig. 4). Thus, the results imply that JFH1-hmAG inherited IFN-sensitivity from JFH1 and that this new infection system is useful for studying mechanisms of IFN actions and viral resistance to IFNs.

In conclusion, we have developed a novel infectious HCV clone (JFH1-hmAG) containing *hmAG* in the NS5A region of the genome,

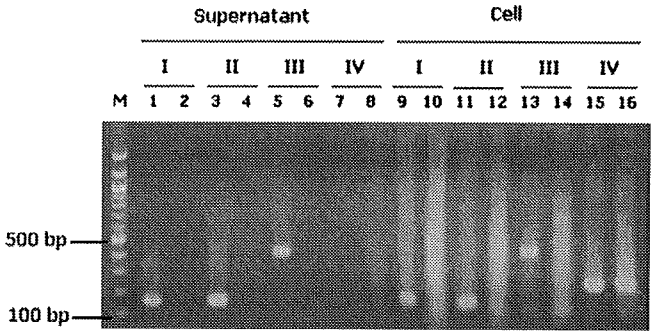

Fig. 3. Reverse transcription (RT) PCR. Huh-7.5.1 cells were inoculated with the supernatant containing JFH1-hmAG virus. Two days after infection, RNA was extracted from cell culture supernatant and from harvested cells. RT-PCRs targeting 5′UTR (group I), NS3 (group II), NS5A-hmAG junction (group III) regions in JFH1-hmAG genome were performed, respectively. RT-PCR targeting GAPDH (group IV) mRNA was also performed simultaneously as a control. Reactions with RNA extracted from culture supernatants (lanes 1, 3, 5, and 7) or cells (lanes 9, 11, 13, and 15) with infection, and from culture supernatants (lanes 2, 4, 6, and 8) or cells (lanes 10, 12, 14, and 16) without infection were shown, respectively.

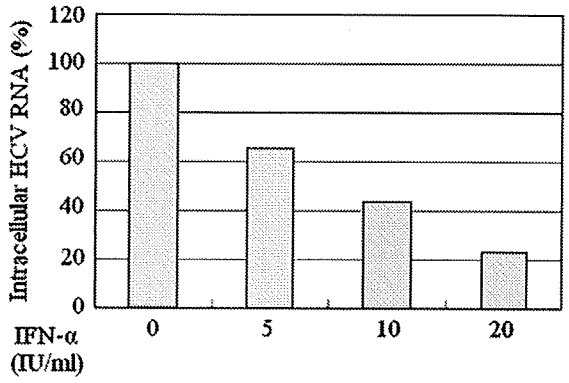

Fig. 4. Inhibition of JFH1-hmAG replication by interferon alpha (IFNα). Huh-7.5.1 cells in duplicate were treated with 0, 5, 10, and 20 U/mL IFNα followed by incubation with the culture supernatant containing with JFH1-hmAG virus. Three days after infection, the relative numbers of intracellular HCV RNA molecules were determined by RT-qPCR (see Materials and methods). Each bar represents the mean number of intracellular HCV RNA molecules expressed as a percentage of that in the control infection without IFN pretreatment.

and have been able to readily observe living infected cells by green-emitting fluorescence. Its replication was restricted by IFNα in a dose-dependent manner. Our results suggested that this new recombinant virus replicated as properly as the parental JFH1 virus, and that this new reporter virus is useful in investigating the HCV biology and the anti-HCV action of IFNs. The JFH1-hmAG virus may provide us with a new system useful for readily screening anti-HCV drugs.

Acknowledgments

We are grateful to Drs. Takaji Wakita and Francis V. Chisari for pJFH1 and Huh-7.5.1, respectively. We thank Drs. Mitsue Hayashi, Zene Matsuda, and Kunito Yoshiike for discussion and encouragement.

W.H. was supported by China Postdoctoral Science Foundation funded project (No. 20070410154). This work was supported by the Program of Founding Research Centers for Emerging and Reemerging Infectious Diseases that was launched as a project commissioned by the Ministry of Education, Culture, Sports, Science and Technology (MEXT), Japan.

References

[1] T. Wakita, T. Pietschmann, T. Kato, T. Date, M. Miyamoto, Z. Zhao, K. Murthy, A. Habermann, H.G. Kräusslich, M. Mizokami, R. Bartenschlager, T.J. Liang, Production of infectious hepatitis C virus in tissue culture from a cloned viral genome, Nat. Med. 11 (2005) 791–796.
[2] J. Zhong, P. Gastaminza, G. Cheng, S. Kapadia, T. Kato, D.R. Burton, S.F. Wieland, S.L. Uprichard, T. Wakita, F.V. Chisari, Robust hepatitis C virus infection in vitro, Proc. Natl. Acad. Sci. USA 102 (2005) 9294–9299.
[3] B.D. Lindenbach, M.J. Evans, A.J. Syder, B. Wölk, T.L. Tellinghuisen, C.C. Liu, T. Maruyama, R.O. Hynes, D.R. Burton, J.A. McKeating, C.M. Rice, Complete replication of hepatitis C virus in cell culture, Science 309 (2005) 623–626.
[4] T. Pietschmann, A. Kaul, G. Koutsoudakis, A. Shavinskaya, S. Kallis, E. Steinmann, K. Abid, F. Negro, M. Dreux, F.L. Cosset, R. Bartenschlager, Construction and characterization of infectious intragenotypic and intergenotypic hepatitis C virus chimeras, Proc. Natl. Acad. Sci. USA 103 (2006) 7408–7413.
[5] M. Yi, Y. Ma, J. Yates, S.M. Lemon, Compensatory mutations in E1, p7, NS2, and NS3 enhance yields of cell culture-infectious intergenotypic chimeric hepatitis C virus, J. Virol. 81 (2007) 629–638.
[6] J.M. Gottwein, T.K. Scheel, A.M. Hoegh, J.B. Lademann, J. Eugen-Olsen, G. Lisby, J. Bukh, Robust hepatitis C genotype 3a cell culture releasing adapted intergenotypic 3a/2a (S52/JFH1) viruses, Gastroenterology 133 (2007) 1614–1626.
[7] T.K. Scheel, J.M. Gottwein, T.B. Jensen, J.C. Prentoe, A.M. Hoegh, H.J. Alter, J. Eugen-Olsen, J. Bukh, Development of JFH1-based cell culture systems for hepatitis C virus genotype 4a and evidence for cross-genotype neutralization, Proc. Natl. Acad. Sci. USA 105 (2008) 997–1002.
[8] M. Yi, R.A. Villanueva, D.L. Thomas, T. Wakita, S.M. Lemon, Production of infectious genotype 1a hepatitis C virus (Hutchinson strain) in cultured human hepatoma cells, Proc. Natl. Acad. Sci. USA 103 (2006) 2310–2315.
[9] R. Bartenschlager, T. Pietschmann, Efficient hepatitis C virus cell culture system: what a difference the host cell makes, Proc. Natl. Acad. Sci. USA 102 (2005) 9739–9740.
[10] R. Bartenschlager, S. Sparacio, Hepatitis C virus molecular clones and their replication capacity in vivo and in cell culture, Virus Res. 127 (2007) 195–207.
[11] R. Bartenschlager, Hepatitis C virus molecular clones: from cDNA to infectious virus particles in cell culture, Curr. Opin. Microbiol. 9 (2006) 416–422.
[12] J.M. Berke, D. Moradpour, Hepatitis C virus comes full circle: production of recombinant infectious virus in tissue culture, Hepatology 42 (2005) 1264–1269.
[13] J. Bukh, R.H. Purcell, A milestone for hepatitis C virus research: a virus generated in cell culture is fully viable in vivo, Proc. Natl. Acad. Sci. USA 103 (2006) 3500–3501.
[14] D. Moradpour, F. Penin, C.M. Rice, Replication of hepatitis C virus, Nat. Rev. Microbiol. 5 (2007) 453–463.
[15] M. Régeard, C. Lepère, M. Trotard, P. Gripon, J. Le Seyec, Recent contributions of in vitro models to our understanding of hepatitis C virus life cycle, FEBS J. 274 (2007) 4705–4718.
[16] P. Sheehy, B. Mullan, I. Moreau, E. Kenny-Walsh, F. Shanahan, M. Scallan, L.J. Fanning, In vitro replication models for the hepatitis C virus, J. Viral Hepat. 14 (2007) 2–10.
[17] T. Suzuki, H. Aizaki, K. Murakami, I. Shoji, T. Wakita, Molecular biology of hepatitis C virus, J. Gastroenterol. 42 (2007) 411–423.
[18] T.L. Tellinghuisen, M.J. Evans, T. von Hahn, S. You, C.M. Rice, Studying hepatitis C virus: making the best of a bad virus, J. Virol. 81 (2007) 8853–8867.
[19] M.B. Zeisel, T.F. Baumert, Production of infectious hepatitis C virus in tissue culture: a breakthrough for basic and applied research, J. Hepatol. 44 (2006) 436–439.
[20] M.P. Manns, G.R. Foster, J.K. Rockstroh, S. Zeuzem, F. Zoulim, M. Houghton, The way forward in HCV treatment—finding the right path, Nat. Rev. Drug Discov. 6 (2007) 991–1000.
[21] K. Moriishi, Y. Matsuura, Evaluation systems for anti-HCV drugs, Adv. Drug Deliv. Rev. 59 (2007) 1213–1221.
[22] J.M. Pawlotsky, S. Chevaliez, J.G. McHutchison, The hepatitis C virus life cycle as a target for new antiviral therapies, Gastroenterology 132 (2007) 1979–1998.
[23] S. Saito, T. Heller, M. Yoneda, H. Takahashi, A. Nakajima, J.T. Liang, Lifestyle-related diseases of the digestive system: a new in vitro model of hepatitis C virion production: application of basic research on hepatitis C virus to clinical medicine, J. Pharmacol. Sci. 105 (2007) 138–144.
[24] T. Wakita, HCV research and anti-HCV drug discovery: toward the next generation, Adv. Drug Deliv. Rev. 59 (2007) 1196–1199.
[25] C.S. Kim, J.H. Jung, T. Wakita, S.K. Yoon, S.K. Jang, Monitoring the antiviral effect of alpha interferon on individual cells, J. Virol. 81 (2007) 8814–8820.
[26] T. Schaller, N. Appel, G. Koutsoudakis, S. Kallis, V. Lohmann, T. Pietschmann, R. Bartenschlager, Analysis of hepatitis C virus superinfection exclusion by using novel fluorochrome gene-tagged viral genomes, J. Virol. 81 (2007) 4591–4603.
[27] D. Moradpour, M.J. Evans, R. Gosert, Z. Yuan, H.E. Blum, S.P. Goff, B.D. Lindenbach, C.M. Rice, Insertion of green fluorescent protein into nonstructural protein 5A allows direct visualization of functional hepatitis C virus replication complexes, J. Virol. 78 (2004) 7400–7409.

[28] S. Karasawa, T. Araki, M. Yamamoto-Hino, A. Miyawaki, A green-emitting fluorescent protein from Galaxeidae coral and its monomeric version for use in fluorescent labeling, J. Biol. Chem. 278 (2003) 34167–34171.
[29] C.N. Stewart Jr., Go with the glow: fluorescent proteins to light transgenic organisms, Trends Biotechnol. 24 (2006) 155–162.
[30] T. Kato, T. Date, A. Murayama, K. Morikawa, D. Akazawa, T. Wakita, Cell culture and infection system for hepatitis C virus, Nat. Protoc. 1 (2006) 2334–2339.
[31] S.B. Kapadia, A. Brideau-Andersen, F.V. Chisari, Interference of hepatitis C virus RNA replication by short interfering RNAs, Proc. Natl. Acad. Sci. USA 100 (2003) 2014–2018.
[32] T. Masaki, R. Suzuki, K. Murakami, H. Aizaki, K. Ishii, A. Murayama, T. Date, Y. Matsuura, T. Miyamura, T. Wakita, T. Suzuki, Interaction of hepatitis C virus nonstructural protein 5A with core protein is critical for the production of infectious virus particles, J. Virol. 82 (2008) 7964–7976.
[33] J. Zhong, P. Gastaminza, J. Chung, Z. Stamataki, M. Isogawa, G. Cheng, J.A. McKeating, F.V. Chisari, Persistent hepatitis C virus infection in vitro: coevolution of virus and host, J. Virol. 80 (2006) 11082–11093.
[34] R. De Francesco, G. Migliaccio, Challenges and successes in developing new therapies for hepatitis C, Nature 436 (2005) 953–960.

PROTEINS
STRUCTURE ■ FUNCTION ■ BIOINFORMATICS

STRUCTURE NOTE

Rhesus macaque: A tight homodimeric CD8αα

Lili Zong,[1,2] Yong Chen,[1,3,4] Hao Peng,[1] Feng Gao,[1] Aikichi Iwamoto,[3,5,6] and George F. Gao[1,3]*

[1] CAS Key Laboratory of Pathogenic Microbiology and Immunology (CASPMI), Institute of Microbiology, Chinese Academy of Sciences (CAS), Beijing 100101, China

[2] Department of Obstetrics and Gynaecology, Zhujiang Hospital, Nanfang Medical University, Guangzhou 510280, China

[3] China-Japan Joint Laboratory of Molecular Immunology and Molecular Microbiology, Institute of Microbiology, Chinese Academy of Sciences (CAS), Beijing 100101, China

[4] College of Life Sciences, Graduate University, Chinese Academy of Sciences (GUCAS), Beijing 100049, China

[5] Research Center for Asian Infectious Diseases, The Institute of Medical Science, The University of Tokyo, Tokyo, Japan

[6] Division of Infectious Diseases, Advanced Clinical Research Center, The Institute of Medical Science, The University of Tokyo, Tokyo, Japan

Key words: rhesus macaque; crystal structure; MHC binding; CD8; dimer; HIV; vaccine.

INTRODUCTION

Simian immunodeficiency virus (SIV) infection of rhesus macaque (*macaca mulatta*) is widely used as an animal model for human immunodeficiency virus (HIV) infection[1–3] as well as other human diseases. It is known that the host cytotoxic T lymphocyte (CTL) responses provide powerful protection against HIV infection, and CTL-based immunization is currently believed to be the most promising approach toward vaccine development.[4]

As a coreceptor of T cell receptor (TCR) on the surface of CTLs, CD8 molecules stabilize the interaction of the TCR with major histocompatibility complex (MHC) by binding to the MHC class I (MHCI) molecule on the surface of antigen-presenting cells. In the absence of CD8 interaction, MHCI-restricted immune responses are hampered.[5] In addition, recent data indicate that CD8 has the ability to bind to a nonclassical MHC class I-like molecule, TL antigen, independently of TCR and CD3, expanding the function of CD8 further to an immunomodulator.[6–8] Moreover, soluble forms of CD8 can disrupt activation of some T cell clones with higher efficacy than anti-CD8 antibodies.[9,10]

In both human and mouse, the functions of CD8 involved in immune responses have been extensively studied.[11,12] The crystal structures of the human HLA-A*0201-CD8αα complex,[13,14] murine MHC H-2K^b-CD8αα complex,[15] TL antigen-CD8αα complex,[16] and the murine CD8αβ heterodimer[17] have been solved. For macaque monkeys, however, little is known on the structures of the CTL-related molecules (e.g., TCR, MHC, and CD8). Only the structure of MHC allele Mamu-A*01 has been recently solved in our laboratory.[18]

In this article, we present the crystal structure of rhesus macaque CD8αα (rCD8αα) homodimer and discuss the relatedness and uniqueness of rCD8αα structure with that of human/mouse CD8αα homodimer. Strikingly, with two Thr43 residues in C–C′ loop, rCD8αα shows a unique extra hydrogen bond in the homodimeric interface indicating a tighter homodimeric interaction.

Grant sponsor: Ministry of Science and Technology (MOST), China (Basic Research Program 973); Grant number: 2006CB504204; Grant sponsor: National Natural Science Foundation (NSFC), China; Grant number: 30671903; Grant sponsor: Chinese Academy of Sciences (CAS, Knowledge Innovation Project); Grant number: KSCX2-SW-227; Grant sponsor: NSFC; Grant number: 30525010; Grant sponsor: Postdoctoral Fund of China; Grant number: 20070410649; Grant sponsor: Japan Ministry of Education, Culture, Sports, Science and Technology (MEXT, The China-Japan Joint Laboratory of Molecular Immunology and Molecular Microbiology).

Lili Zong and Yong Chen contributed equally to this work.

*Correspondence to: George F. Gao, Center for Molecular Immunology, Institute of Microbiology, Chinese Academy of Sciences (CAS), Datun Road, ChaoYang District, Beijing 100101, China. E-mail: gaof@im.ac.cn

Received 28 September 2008; Revised 10 November 2008; Accepted 12 November 2008

Published online 19 November 2008 in Wiley InterScience (www.interscience.wiley.com). DOI: 10.1002/prot.22331

© 2008 WILEY-LISS, INC.

MATERIALS AND METHODS

Expression and purification of rCD8αα homodimer

Rhesus macaque CD8 (rCD8) alpha chain nucleotides covering amino acids 1–120 of the ectodomain were synthesized based on the sequence of Indian origin rhesus (GeneBank ID: 698329). Inclusion bodies of rCD8α were prepared, and rCD8αα homodimer was renatured and purified by using the protocols described earlier.[13,14]

Crystallization, data collection, and processing

All crystallization attempts were performed at 18°C by the hanging drop vapor diffusion method. Ideal rCD8αα crystals grew from a 1:1 mixture of the protein solution (10 mg/mL) with crystallization reagent of 0.05*M* potassium phosphate monobasic, 20% w/v polyethylene glycol 8000. Data were collected using a Rigaku MicroMax007 rotating-anode X-ray generator (Cu Kα; λ = 1.5418 Å) equipped with an R-AXIS VII++ image-plate detector. Data were processed and scaled using HKL2000.[19]

Structure solution, refinement, and analysis

Data were analyzed by molecular replacement[20] using Molrep in the CCP4 package,[21] taking human CD8αα as the search probe (PDB code: 1AKJ).[14] Final rounds of refinement resulted in a final Rcryst of 21.3% (R_{free} = 25.7%) for all data between 35.0 and 2.20 Å.

Buried surface areas were calculated using SURFACE[21] with a 1.4 Å probe radius. The PyMOL Molecular Graphics System (DeLano Scientific, http://www.pymol.org) was used to prepare figures. Geometry of the refined structure was validated according to Ramachandran plot criteria.[22] The data collection and refinement statistics of the structure are shown in Table I.

Accession number

Atomic coordinates of rhesus macaque CD8αα homodimer have been deposited in the Protein Data Bank (PDB, http://www.rcsb.org/pdb) under accession code: 2Q3A.

RESULTS AND DISCUSSION

Overall structure of rhesus macaque CD8αα homodimer

The crystals contained two CD8αα molecules as a dimer in a hand-shaking mode per crystallographic asymmetric unit. Belonging to the V set of Ig folds,[14] the overall structure comparison of rCD8αα homodimer with the human counterpart is shown in Figure 1(A).

Table I
X-Ray Diffraction Data Processing and Refinement Statistics

Data collecting	
Space group	$P2_12_12_1$
Unit cell dimensions (*a*, *b*, *c*)	46.54, 56.26, 82.31
Unit cell dimensions (α, β, γ)	90.00, 90.00, 90.00
Resolution range (Å)	40.00–2.20 (2.32–2.20)[a]
Total number of reflections	138,752
Number of unique reflections	17,807
Number of molecule in the asymmetric unit	2
Average redundancy	6.60 (5.90)
Completeness (%)	99.6 (100.0)
R_{merge} (%)	9.6 (29.5)
I/σ	12.8 (5.7)
Refinement	
Resolution (Å)	35.85–2.20
R-factor (%)	21.3
R_{free}[b] (%)	25.7
RMS deviations from restraint target values:	
Bond lengths (Å)	0.006
Bond angles (°)	1.33
Ramachandran plot Quality:	
Residues in most favored regions	165 [84.2%]
Residues in additional allowed	27 [13.8%]
Residues in generously allowed	4 [2.0%]
Residues in disallowed regions	0 [0%]

[a]Values in parentheses are given for the highest resolution shell.
[b]R_{free} is calculated over reflections in a test set (5%) not included in atomic refinement.

Each CD8α molecule is primarily composed of β structure arranged into two antiparallel β sheets. Short regions of 3_{10} helix are found between the E and F strands, which are not commonly found in CD8β molecules.

All residues corresponding to the HLA-A2-CD8αα interface remain the same in MHC Mamu-A*01 and rCD8αα.[18] The interaction of HLA-CD8 is mainly based on charge complementarity and exhibits relatively low affinity (KD = 100–223 μ*M*) and rapid kinetics.[8,23] The molecular surfaces of Mamu-A*01 and rCD8αα show similar complementarities (data not shown), indicating their interaction.

Structural comparison of rhesus macaque with human or murine CD8αα homodimer

Superposition of the final structure of rCD8αα dimer shows closer resemblance to human CD8αα homodimer (1AKJ, in complex with HLA-A2)[14] than to murine CD8αα (mCD8αα) (1BQH, in complex with Kd)[15] [Fig. 1(A,B)]. Root mean square deviation (RMSD) of rCD8αα and hCD8αα dimer results in 0.831 E for all Cα atoms, which is much smaller than that of rCD8αα with mCD8 dimer of 1.634 E.

The comparison of r/h/m CD8αα reveals some differences in loop regions, especially in complementarity

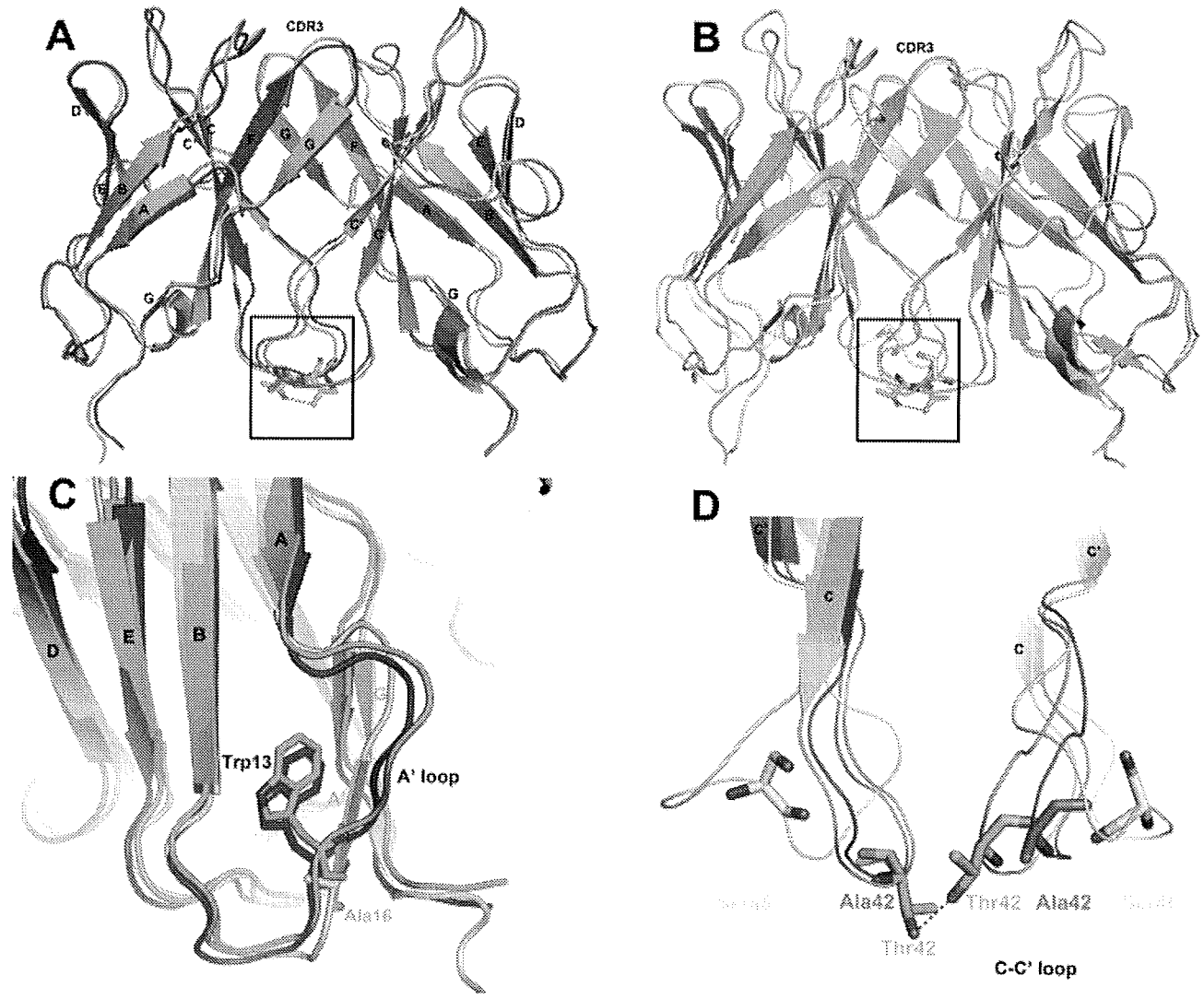

Figure 1

Crystal structure of rCD8αα homodimer and its superposition with human and mouse CD8αα structures. The ribbon diagram of each CD8αα was drawn and color-coded as: rCD8αα, green and cyan; hCD8αα, blue and magenta; mCD8αα, yellow and orange. (**A**) Superposition of rCD8αα and hCD8αα. The extra hydrogen bond region of rCD8αα was boxed. (**B**) Superposition of rCD8αα and mCD8αα. The extra hydrogen bond region of rCD8αα was boxed. (**C**) The transition of A'-β strand in mCD8αα and A' loop in both rCD8αα/hCD8αα as the residue changes (Ala16 to Trp13). (**D**) Thr43 residues in C-C' loop of rCD8αα homodimer (cyan) form extra hydrogen bonds. Hydrogen bond between two main-chains is shown as red dashed line.

determining regions (CDRs), which are involved in MHCIs binding. Interestingly, though CDR1 and CDR2 are structurally variable, CDR3 has almost the same conformation among r/h/m CD8αα molecules [Fig. 1(A,B)].

As one of the elements commonly found in many Ig domains, the first β strand of each domain is split into two shorter strands (A and A′).[20] rCD8αα homodimer can also be characterized by a *cis*-proline (Pro7) at the transition point at the A strand. However, at the place of the A′ strand, a loop is located in rhesus macaque as well as human CD8α molecules as the result of the big side chain of the residue Trp13, which is equivalent to Ala16 in mCD8α molecules [Fig. 1(C)].

Corresponding to Ala42 in hCD8α and Ser48 in mCD8α, Thr43 residues in rCD8α form an additional hydrogen bond to each other. This extra H-bond enhances the dimeric interaction and brings the C–C′ loop of the two molecules into a much closer position [Fig. 1(D)]. As a result, the interface size of the two rCD8α subunits (~2274 Å^2, total buried solvent-accessible surface area) is significantly larger than that of human CD8α interface (~2038 Å^2) indicating a tighter homodimeric interaction of CD8αα in rhesus macaque.

ACKNOWLEDGMENTS

The authors thank Dr. Fuliang Chu for his valuable suggestions for this project and Mr. Christopher Pannell for his critical reading of the manuscript.

REFERENCES

1. Allen TM, Sidney J, del Guercio MF, Glickman RL, Lensmeyer GL, Wiebe DA, DeMars R, Pauza CD, Johnson RP, Sette A, Watkins DI. Characterization of the peptide binding motif of a rhesus MHC class I molecule (Mamu-A*01) that binds an immunodominant CTL epitope from simian immunodeficiency virus. J Immunol 1998;160:6062–6071.
2. Matano T, Shibata R, Siemon C, Connors M, Lane HC, Martin MA. Administration of an anti-CD8 monoclonal antibody interferes with the clearance of chimeric simian/human immunodeficiency virus during primary infections of rhesus macaques. J Virol 1998;72:164–169.
3. Schmitz JE, Kuroda MJ, Santra S, Sasseville VG, Simon MA, Lifton MA, Racz P, Tenner-Racz K, Dalesandro M, Scallon BJ, Ghrayeb J, Forman MA, Montefiori DC, Rieber EP, Letvin NL, Reimann KA. Control of viremia in simian immunodeficiency virus infection by CD8+ lymphocytes. Science 1999;283:857–860.
4. Kaufmann SH, McMichael AJ. Annulling a dangerous liaison: vaccination strategies against AIDS and tuberculosis. Nat Med 2005;11: S33–S44.
5. Fung-Leung WP, Schilham MW, Rahemtulla A, Kundig TM, Vollenweider M, Potter J, van Ewijk W, Mak TW. CD8 is needed for development of cytotoxic T cells but not helper T cells. Cell 1991;65:443–449.
6. Cole DK, Gao GF. CD8: adhesion molecule, co-receptor and immuno-modulator. Cell Mol Immunol 2004;1:81–88.
7. Leishman AJ, Naidenko OV, Attinger A, Koning F, Lena CJ, Xiong Y, Chang HC, Reinherz E, Kronenberg M, Cheroutre H. T cell responses modulated through interaction between CD8αα and the nonclassical MHC class I molecule, TL. Science 2001;294:1936–1939.
8. Wyer JR, Willcox BE, Gao GF, Gerth UC, Davis SJ, Bell JI, van der Merwe PA, Jakobsen BK. T cell receptor and coreceptor CD8 αα bind peptide-MHC independently and with distinct kinetics. Immunity 1999;10:219–225.
9. Cole DK, Rizkallah PJ, Boulter JM, Sami M, Vuidepot AL, Glick M, Gao F, Bell JI, Jakobsen BK, Gao GF. Computational design and crystal structure of an enhanced affinity mutant human CD8 αα coreceptor. Proteins 2007;67:65–74.
10. Sewell AK, Gerth UC, Price DA, Purbhoo MA, Boulter JM, Gao GF, Bell JI, Phillips RE, Jakobsen BK. Antagonism of cytotoxic T-lymphocyte activation by soluble CD8. Nat Med 1999;5:399–404.
11. Gao GF, Jakobsen BK. Molecular interactions of coreceptor CD8 and MHC class I: the molecular basis for functional coordination with the T-cell receptor. Immunol Today 2000;21:630–636.
12. Gao GF, Rao Z, Bell JI. Molecular coordination of αβ T-cell receptors and coreceptors CD8 and CD4 in their recognition of peptide-MHC ligands. Trends Immunol 2002;23:408–413.
13. Gao GF, Gerth UC, Wyer JR, Willcox BE, O'Callaghan CA, Zhang Z, Jones EY, Bell JI, Jakobsen BK. Assembly and crystallization of the complex between the human T cell coreceptor CD8α homodimer and HLA-A2. Protein Sci 1998;7:1245–1249.
14. Gao GF, Tormo J, Gerth UC, Wyer JR, McMichael AJ, Stuart DI, Bell JI, Jones EY, Jakobsen BK. Crystal structure of the complex between human CD8α(α) and HLA-A2. Nature 1997;387:630–634.
15. Kern PS, Teng MK, Smolyar A, Liu JH, Liu J, Hussey RE, Spoerl R, Chang HC, Reinherz EL, Wang JH. Structural basis of CD8 coreceptor function revealed by crystallographic analysis of a murine CD8αα ectodomain fragment in complex with H-2Kb. Immunity 1998;9:519–530.
16. Liu Y, Xiong Y, Naidenko OV, Liu JH, Zhang R, Joachimiak A, Kronenberg M, Cheroutre H, Reinherz EL, Wang JH. The crystal structure of a TL/CD8αα complex at 2.1 A resolution: implications for modulation of T cell activation and memory. Immunity 2003;18:205–215.
17. Chang HC, Tan K, Ouyang J, Parisini E, Liu JH, Le Y, Wang X, Reinherz EL, Wang JH. Structural and mutational analyses of a CD8αβ heterodimer and comparison with the CD8αα homodimer. Immunity 2005;23:661–671.
18. Chu F, Lou Z, Chen YW, Liu Y, Gao B, Zong L, Khan AH, Bell JI, Rao Z, Gao GF. First glimpse of the peptide presentation by rhesus macaque MHC class I: crystal structures of Mamu-A*01 complexed with two immunogenic SIV epitopes and insights into CTL escape. J Immunol 2007;178:944–952.
19. Otwinowski Z, Minor W. Processing of X-ray diffraction data collected in oscillation mode. Methods Enzymol 1997;276:307–326.
20. Chen Y, Chu F, Gao F, Zhou B, Gao GF. Stability engineering, biophysical, and biological characterization of the myeloid activating receptor immunoglobulin-like transcript 1 (ILT1/LIR-7/LILRA2). Protein Expr Purif 2007;56:253–260.
21. CCP4. The CCP4 suite: programs for protein crystallography. Acta Crystallogr D Biol Crystallogr 1994;50:760–763.
22. Lovell SC, Davis IW, Arendall WB, III, de Bakker PI, Word JM, Prisant MG, Richardson JS, Richardson DC. Structure validation by Cα geometry: π,ψ and Cβ deviation. Proteins 2003;50:437–450.
23. Gao GF, Willcox BE, Wyer JR, Boulter JM, O'Callaghan CA, Maenaka K, Stuart DI, Jones EY, Van Der Merwe PA, Bell JI, Jakobsen BK. Classical and nonclassical class I major histocompatibility complex molecules exhibit subtle conformational differences that affect binding to CD8αα. J Biol Chem 2000;275:15232–15238.

Analytical Biochemistry 385 (2009) 278–285

Contents lists available at ScienceDirect

Analytical Biochemistry

journal homepage: www.elsevier.com/locate/yabio

Thermus thermophilus-derived protein tags that aid in preparation of insoluble viral proteins

Naoyuki Kondo [a,b], Akio Ebihara [c,1], Heng Ru [b], Seiki Kuramitsu [c,d], Aikichi Iwamoto [a,e], Zihe Rao [b,f], Zene Matsuda [a,b,*]

[a] *Research Center for Asian Infectious Diseases, Institute of Medical Science, University of Tokyo, 4-6-1, Shirokanedai, Minato-ku, Tokyo 108-8639, Japan*
[b] *China–Japan Joint Laboratory of Structural Virology and Immunology, Institute of Biophysics, Chinese Academy of Sciences, Beijing 100101, People's Republic of China*
[c] *RIKEN SPring-8 Center, Harima Institute, Hyogo 679-5148, Japan*
[d] *Department of Biological Sciences, Graduate School of Science, Osaka University, Osaka 560-0043, Japan*
[e] *Division of Infectious Diseases, Advanced Clinical Research Center, Institute of Medical Science, University of Tokyo, Tokyo 108-8639, Japan*
[f] *National Laboratory of Biomacromolecules, Institute of Biophysics, Chinese Academy of Sciences, Beijing 100101, People's Republic of China*

ARTICLE INFO

Article history:
Received 1 September 2008
Available online 19 November 2008

Keywords:
Thermus thermophilus
HIV
Protein tag
Solubilization
Vpr
Membrane-spanning domain

ABSTRACT

The expression and solubilization of insoluble proteins have been facilitated by the introduction of protein tags. In our analyses of viral protein R (Vpr) of human immunodeficiency virus 1 (HIV-1), however, several conventional tag proteins enhanced its expression but failed to solubilize it. Therefore, we decided to explore whether proteins derived from *Thermus thermophilus* HB8 (*T. th.*), a highly heat-stable bacterium, could be used as tag proteins to enhance the solubilization of Vpr. Based on the data accumulated during the recent structural genomics project of *T. th.*, we selected 15 *T. th.* proteins with high expression levels and solubilities. From this group, we identified a *T. th.* tag protein that expressed Vpr in a soluble form. Furthermore, two *T. th.* tag proteins, including the identified one, were found to solubilize the extremely insoluble membrane-spanning domain of the envelope protein of HIV-1. When green fluorescent protein (GFP) was used as a passenger protein of *T. th.* tags, the brightness and stability of GFP were similar to those of untagged GFP, suggesting that the *T. th.* tags do not negatively affect the function of the passenger protein. Thus, data of structural genomics can be applied to generate a customized versatile protein tag for protein analyses.

© 2008 Elsevier Inc. All rights reserved.

The structures of various proteins have been determined during recent years, owing mainly to the progress of structural genomics (SG)[2] research. This information not only enriches our knowledge of certain aspects of basic protein science, such as protein-folding patterns and specific protein–protein interactions, but also provides practical contributions for structure-oriented drug design against pathogens [1–5]. The structures of some proteins remain unknown, however, because the proteins have unfavorable properties that hinder attempts to analyze their structures. Such properties include low expression level, low solubility, difficulty of purification, poor crystallizability, and instability of formed crystals. Adaptor proteins that interact with multiple other proteins, or membrane proteins with highly hydrophobic segments, often possess these properties.

The use of certain tag proteins can overcome some of these problems. A small peptide tag such as a polyhistidine tag, for example, can facilitate both the detection and purification of a target protein [6,7]. Some larger peptide tags (or protein tags) can likewise improve detection and purification while also enhancing the expression level and solubility of a protein of interest. Indeed, maltose binding protein (MBP) [8], glutathione *S*-transferase (GST) [9], thioredoxin (TRX) [10], and N utilization substance A (NusA) [11] have been widely used, and several expression vectors are commercially available. Several groups have compared the efficiency of conventional tag proteins for expression [12–15]. Although each of these studies used different expression vectors and passenger proteins, it seems reasonable to conclude that one should try several tag proteins for a particular passenger protein because the potency of a tag can be affected by multiple factors,

* Corresponding author. Address: Research Center for Asian Infectious Diseases, Institute of Medical Science, University of Tokyo, 4-6-1, Shirokanedai, Minato-ku, Tokyo 108-8639, Japan. Fax: +81 3 6409 2208.
E-mail address: zmatsuda@ims.u-tokyo.ac.jp (Z. Matsuda).
[1] Present address: Laboratory of Applied Biochemistry, Faculty of Applied Biological Sciences, Gifu University, Gifu 501-1193, Japan.

[2] *Abbreviations used:* SG, structural genomics; MBP, maltose binding protein; GST, glutathione *S*-transferase; TRX, thioredoxin; NusA, N utilization substance A; HIV, human immunodeficiency virus; SIV, simian immunodeficiency virus; AIDS, acquired immunodeficiency syndrome; Vpr, virus protein R; MSD, membrane-spanning domain; *T. th.*, *Thermus thermophilus;* GFP, green fluorescent protein; Vpx, viral protein X; PCR, polymerase chain reaction; LB, Luria–Bertani; IPTG, isopropylthiogalactoside; SDS–PAGE, sodium dodecyl sulfate–polyacrylamide gel electrophoresis; PBS, phosphate-buffered saline; GdmHCl, guanidium hydrochloride; CD, circular dichroism; UV, ultraviolet; FACS, fluorescence-activated cell sorting.

0003-2697/$ - see front matter © 2008 Elsevier Inc. All rights reserved.
doi:10.1016/j.ab.2008.10.050

including the specific properties of the passenger proteins as well as the linker between the tag and passenger proteins.

In many cases, tag proteins serve as molecular chaperons during the synthesis and folding of the passenger protein [12], only to be removed after production and purification. For an extremely insoluble passenger protein, a tag protein is retained so as to facilitate solubilization. If a proper tag protein is selected, the passenger protein's function is well maintained even with a fused tag form [16]. Moreover, the remaining tag proteins, if their structures are known, can serve as models of molecular replacement for phase determination [16,17]. Lysozyme [18], MBP [19], and GST [20] have been successfully used for this purpose.

In our laboratory, we are studying the several proteins of primate lentiviruses, human immunodeficiency virus (HIV), and simian immunodeficiency virus (SIV) that are linked with acquired immunodeficiency syndrome (AIDS). One of them is virus protein R (Vpr), and another is gp41, a subunit of envelope protein. Vpr is a highly insoluble 14-kDa accessory gene product of HIV-1. It works as a pleiotropic adaptor protein in the life cycle of HIV-1 [21–26]. The gp41 subunit plays a critical role for membrane fusion and contains highly hydrophobic membrane-spanning domain (MSD). The membrane-spanning domain of gp41 (gp41-MSD) anchors the HIV-1 envelope protein to lipid bilayers [27]. During our study of these insoluble proteins, we tried to improve solubilization by using several conventional tag proteins but had limited success. Therefore, we tried to identify new tag proteins that would facilitate the production and structure determination of proteins of interest. We sought candidate tag proteins from *Thermus thermophilus* (*T. th.*), one of the well-characterized model organisms of the SG project [28,29]. Because *T. th.* survives at 85 °C and its proteins are heat-stable [30], the structures of more than 400 of approximately 2000 known gene products have been determined during the past 5 years [28]. Drawing on information that has accumulated from SG research on *T. th.* proteins, we tested proteins with high expression and solubility characteristics and known high-resolution three-dimensional structures for their utility as candidate tag proteins.

We tested 15 candidate tag proteins on Vpr of HIV-1 and identified a *T. th.* tag protein that could express a soluble form of Vpr. This tag and another tag were also able to help expression of a gp41-MSD. Analyses using green fluorescent protein (GFP) as a fusion passenger protein suggested that these *T. th.* tags did not significantly affect the biophysical properties of the passenger proteins. Our results suggest that the information accumulated during the SG project, as exemplified here for *T. th.*, can be a versatile resource for the identification of customized tag proteins that may facilitate biophysical and structural analyses of highly insoluble proteins.

Materials and methods

Selection of candidate tag proteins from T. th

We used the accumulated data from expression, purification, and crystallization trials in the Whole Cell Project of *T. th.* [29,31] to select candidate proteins. From the more than 400 proteins with known structures, we selected proteins that showed good expression and solubility. In the Whole Cell Project of *T. th.*, we arbitrarily defined seven classes to indicate a protein's expression level and solubility fitness: (i) no expression, (ii) low expression and low solubility, (iii) high expression and low solubility, (iv) high expression and half solubility, (v) low expression and high solubility, (vi) high expression and half solubility, and (vii) high expression and high solubility. We selected proteins that fell in the high expression and high solubility category. Among these selected proteins, we further narrowed the field by choosing candidates whose resolution of the determined structure is higher than 2 Å.

Construction of expression plasmids

All of the proteins were expressed in *Escherichia coli* BL21 Star (DE3) (Invitrogen) using the same plasmid derived from pET-47b (Novagen). pET-47b contains a T7 promoter, a six polyhistidine tag-coding sequence, and an HRV 3C protease recognition sequence upstream of the multiple cloning site. A tag protein was added at either the N or C terminus of a passenger protein (Fig. 1). To add the tag at the N terminus, we used a modified pET-47b plasmid called pET-47md that had been produced by cloning an oligonucleotide cassette with *Asc*I, *Pac*I, *Bam*HI, and *Bsr*GI sites, in that order, between the *Kpn*I and *Avr*II sites of pET-47b. To fuse a candidate tag protein at the C terminus of a passenger protein, pET-47b was used. The pET-47b vector has *Bam*HI, *Bsr*GI, *Asc*I, and *Pac*I sites, in that order, in the multiple cloning site.

The genes for tag proteins were amplified by polymerase chain reaction (PCR) using primers that contained *Asc*I and *Pac*I sites at the 5′ and 3′ termini of the genes while also using KOD Plus (Toyobo), Pfu Turbo (Stratagene), and Ex Taq (Takara) DNA polymerases. The template DNAs we used included 15 *T. th.* expression plasmids for *T. th.* genes [31,32] (RIKEN Bioresource Center DNA bank), pMALp2e (New England Biolabs) for *mbp*, pGEX5x-1 (GE Healthcare) for *gst*, pET-50b (Novagen) for *nusA*, pSP65HXB2gpt for *vpr*, and the synthetic *vpx* (viral protein X) gene whose sequence is based on that of SIVmac251 and optimized for yeast codon use. Modified GFPs, which were used as passenger proteins, were also amplified by PCR using primers with *Bam*HI and *Bsr*GI sites at the 5′ and 3′ termini, respectively [33]. The MSD portion of gp41 [27] was synthesized as a complementary pair of oligode-

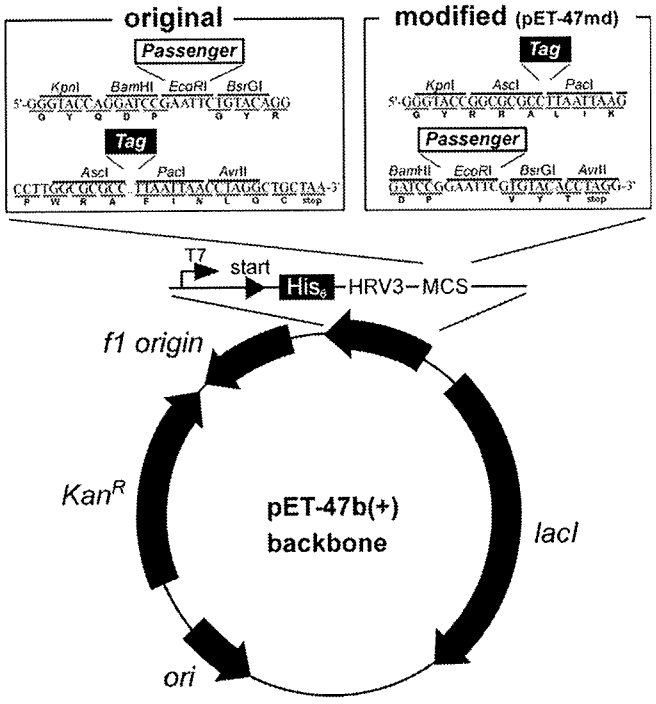

Fig. 1. Schematic representation of plasmids used in this study. The upper panel shows the details of the multiple cloning site of pET-47b and pET-47md. The lower panel shows the structure of the backbone. T7, T7 promoter; His_6, polyhistidine tag; HRV3, region coding amino acid sequences recognized by HRV 3C protease; MCS, multiple cloning site; Tag, genes of tag proteins; Passenger, genes of passenger proteins.

oxyribonucleotides with *Bam*HI and *Bsr*GI sites at the 5′ and 3′ termini, respectively. All amplicons were first cloned into pCR4blunt-TOPO vectors using the TOPO Cloning Kit (Invitrogen), and their sequences were verified before being cloning into pET-47b or pET-47md. After cloning the individual passenger gene between the *Bam*HI and *Bsr*GI sites of pET-47b or pET-47md, the respective tag genes were cloned using the *Asc*I and *Pac*I sites. As a control, we constructed expression vectors containing tag genes but without passenger genes; this was accomplished by cloning the tag genes to pET-47md with the *Asc*I and *Pac*I sites. We verified all sequences of the constructed expression vectors.

Analysis of protein expression on a small-scale

BL21 Star (DE3) (Invitrogen) was transformed by the constructed expression plasmids and cultured on Luria–Bertani (LB) plates containing 50 μg/ml kanamycin. Fresh colonies were picked and inoculated into 2 ml of LB medium containing 50 μg/ml kanamycin. All *E. coli* cells were grown at 37 °C throughout the experiments. When the cells had reached a log phase, isopropylthiogalactoside (IPTG) was added in a final concentration of 1 mM. After a 5-h growth period, the cells were harvested by centrifuging at 15,000g for 10 min at 4 °C using an MX-301 centrifuge (Tomy). We extracted the expressed proteins using 300 μl of BugBuster (Novagen) that contained 0.3 μl of Benzonase (Novagen). The total lysate and supernatant was subjected to sodium dodecyl sulfate–polyacrylamide gel electrophoresis (SDS–PAGE) using a 5% to 20% SDS gradient gel (DRC). We confirmed the expressed protein with the peptide mass fingerprinting method using AXIMA–CFR Plus (Shimadzu).

Measurement of fluorescent activity of GFP

BL21 Star (DE3) cells that had been transformed using the GFP expression vectors (GFP alone or tag-fused GFP at the N terminus) were grown for 5 h in LB medium containing 1 mM IPTG and then harvested by centrifugation (15,000g, 4 °C). The cell pellets were suspended in 0.7 ml of phosphate-buffered saline (PBS), and the optical densities at 600 nm were determined. The fluorescence of the suspended cells was analyzed using a FACSCalibur flow cytometer (BD Biosciences). We normalized the measured mean fluorescence signal by dividing it by the obtained optical densities at 600 nm (OD_{600}).

Analysis of stability of tagged protein

A 20-μl aliquot of the supernatant of tag-free or tag-fused GFP-expressing cell lysate prepared as described above was added to a 500-μl buffer solution containing 20 mM Tris–HCl (pH 8.0) and increasing concentrations (1, 2, 3, 4, and 5 M) of guanidium hydrochloride (GdmHCl). After incubating the preparations for 1 day at room temperature, we measured the emission spectra from 500 to 600 nm using an F-4500 fluorescence spectrophotometer (Hitachi) set to an excitation wavelength of 470 nm.

Large-scale expression and purification

BL21 Star (DE3) cells transformed with individual expression plasmids were grown in 1 L of LB medium containing 50 μg/ml kanamycin. When OD_{600} reached 0.5 to 0.7, IPTG was added to produce a final concentration of 1 mM so as to induce the expression of target proteins. After a 5-h growth period, cells were pelleted down and frozen at −30 °C. To extract the protein, the cell pellets were resuspended in buffer A (20 mM NaPi [pH 7.4], 0.5 M NaCl, and 20 mM imidazole). The suspended cells were placed on ice and subjected to ultrasonication for 1 h. The disrupted cell extract was centrifuged at 5000g for 30 min at 4 °C to remove insoluble materials. The supernatants were loaded onto Ni Sepharose 6 Fast Flow columns (GE Healthcare) and eluted with a second buffer (20 mM NaPi [pH 7.4], 0.5 M NaCl, and 0.5 M imidazole). HRV 3 C protease (Novagen) was added to the eluted fractions, and the preparations were incubated at 4 °C for more than 16 h to remove the polyhistidine tags. After exchanging the second buffer for buffer A using VivaSpin (Sartorius), the solutions again were loaded onto Ni Sepharose 6 Fast Flow columns. The flow-through fraction was collected and concentrated to 2 to 5 ml in a buffer containing 50 mM Tris–HCl (pH 8.0) and 0.5 M NaCl. The concentrated fraction was subjected to Superdex 200 size exclusion chromatography using an AKTA Purifier (GE Healthcare). We collected the highest peaks and verified their content using SDS–PAGE.

Secondary structure analyses

Purified proteins were placed in buffer (20 mM NaPi [pH 7.0] and 0.5 M NaCl), and their circular dichroism (CD) in the far-UV (ultraviolet) region of 200 to 250 nm was measured at 25 °C using a Pistar-180 Spectrometer (Applied Photophysics).

Results

Expression of Vpr protein with conventional tag fusion

To obtain soluble Vpr protein for future analysis, we tried to express Vpr in *E. coli*. When Vpr was expressed without any tag, it did not express very well. Even when it was expressed, it did not come to a soluble fraction (Fig. 2A). This is consistent with previous studies [26,34]. The conventional tag genes *mbp*, *gst*, and *nusA* were introduced upstream or downstream of the HIV *vpr* gene in the expression plasmid (Fig. 1). Among the conventional tag proteins, GST and NusA facilitated expression of fusion protein when added at the N or C terminus, whereas MBP failed to achieve a high expression level (Fig. 2B). Unfortunately, all of the tagged Vpr proteins that were expressed were observed in the insoluble fraction (Fig. 2B).

Selection of candidate T. th. tag protein

To seek other effective tags for Vpr protein expression and solubilization, we decided to introduce proteins from *T. th.*; the SG project of *T. th.* [28] has provided many data sets, including those for protein expression, purification, and crystallization [29], that aided in our selection of viable candidates for this effort. We selected 59 candidates from more than 400 proteins based on their expression level and the solubility (see Materials and methods for details). From these 59, we selected 31 candidates with resolutions of structures higher than 2 Å. By coincidence, the molecular weight of each of the 31 candidates was less than 40 kDa. This may reflect the fact that smaller molecular weight proteins are easier to express and crystallize [35].

We further narrowed the candidate pool by selecting 14 proteins for which information on small-scale protein preparation was available. To these 14 candidates, we added a 57.9-kDa protein, the largest in the first-pass group of 59 proteins. We included this protein so as to have a larger molecular weight tag protein that could serve as a favorable model of molecular replacement for larger passenger proteins. The complete list of 15 candidate proteins appears in Table 1. As a group, there seemed to be no common functional or structural correlations, probably because we selected the candidates solely for their practical properties of expression and solubility and on their structural analyses.

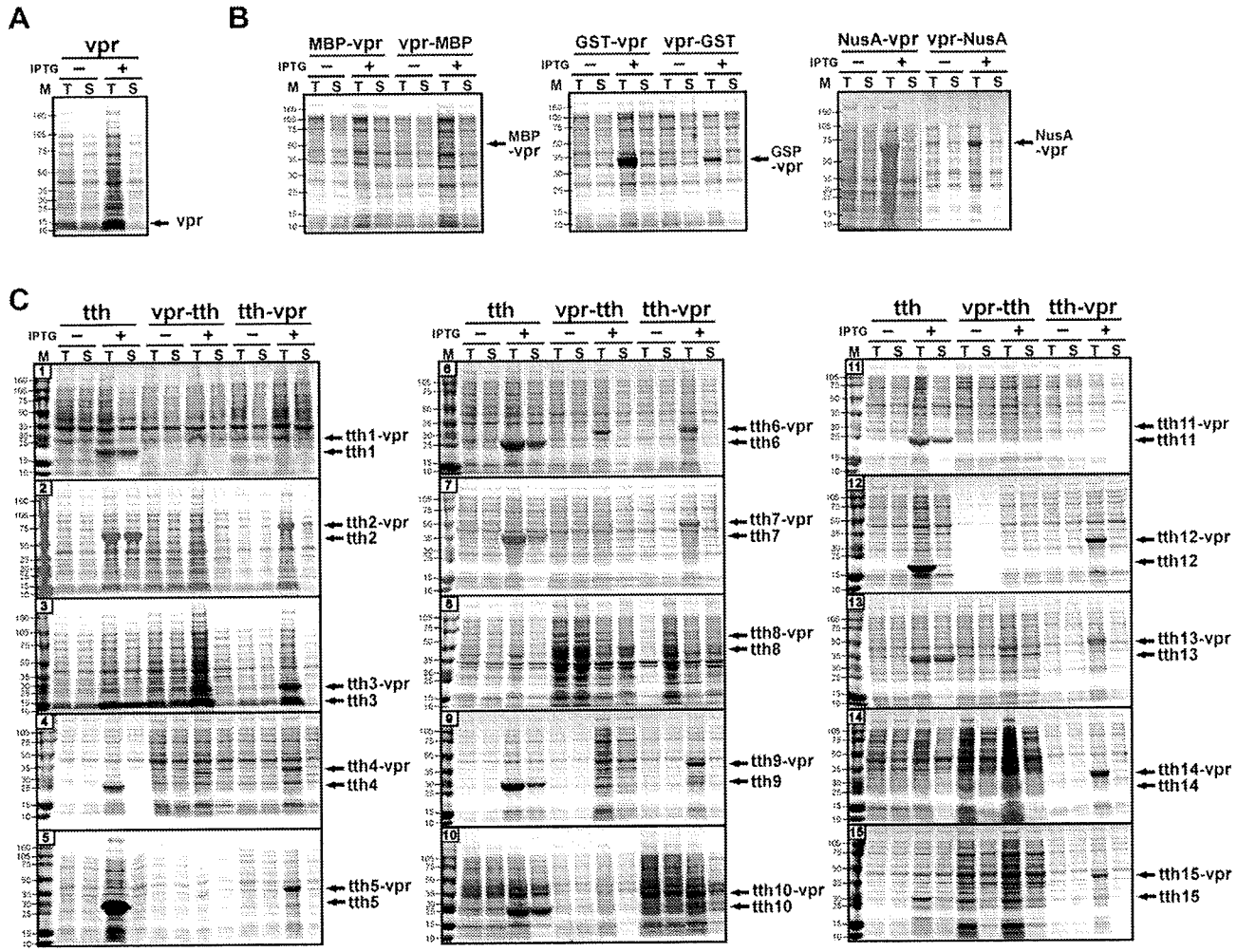

Fig. 2. Expression profile of tag protein-fused Vpr with (+) or without (−) induction by IPTG. Based on calculated molecular weights, the positions of expected proteins are marked by arrows along the right edge of each gel. (A) Expression profiles of tag-free Vpr. (B) Expression profiles of MBP-fused Vpr, GST-fused Vpr, and NusA-fused Vpr. (C) Expression profiles of individual *T. th.* protein candidates alone (tth) and when fused with Vpr at the C terminus (vpr–tth) or at the N terminus (tth–vpr). The number indicated in the box in the upper left corner of each gel corresponds to the number used for the candidate tth gene listed in Table 1. Gel columns indicate molecular weight markers (in kDa) (M), total lysate (T), and supernatant (S).

Table 1
Selected candidates of protein tags from *T. th.*

Name in this study	Locus tag in genome	Functional feature	M_W (kDa)	PDB ID	Resolution (Å)
tth1	TTHA0132	Conserved hypothetical protein	16.9	2dx6	1.78
tth2	TTHA0271	Molecular chaperon, GroEL	57.9	1wf4	2.80
tth3	TTHA0281	UPF0150 family protein	9.8	2dsy	1.90
tth4	TTHA0341	Molybdopterin biosynthesis enzyme MoaB	17.8	2is8	1.64
tth5	TTHA1053	Conserved hypothetical protein	20.7	2cve	1.60
tth6	TTHA1091	Conserved hypothetical protein	17.8	1vgg	1.75
tth7	TTHA1199	Ornithine carbamoyltransferase	33.3	2ef0	2.00
tth8	TTHA1275	C subunit of $V_1 - V_0$ ATPase	36.0	1v9m	1.85
tth9	TTHA1359	Transcriptional regulator	22.4	2zcw	1.50
tth10	TTHA1671	Adenylate kinase	20.7	3cm0	1.80
tth11	TTHA1699	Putative transediting enzyme of tRNA-Syn	16.6	2cx5	1.90
tth12	TTHA1713	Conserved hypothetical protein	14.4	2cu5	1.84
tth13	TTHA1838	Atypical ABC-ATPase, SufC	27.6	2d2f	1.90
tth14	TTHA1897	GidA-related protein	25.9	2cul	1.65
tth15	TTHB192	CRISPR-associated protein	23.8	1wj9	1.90

Expression of Vpr protein with T. th. protein fusion

Because the expression vectors used in this study (pET-47b and pET-47md) (Fig. 1) have the polyhistidine and protease recognition sequences that are absent from the vectors used in the *T. th.* SG project (pET-3a and pET-11a) [28,29], we began our investigation by evaluating the selected *T. th.* proteins in the pET-47b backbone. Our results showed that although all *T. th.* proteins were expressed well, 7 of the 15 *T. th.* proteins (Tth4, Tth5, Tth7, Tth8, Tth12, Tth14, and Tth15) failed to solubilize (Fig. 2C, tth). Because the general

conditions for the expression, such as growth medium, growth temperature (37 °C), and IPTG concentration, were identical to those of the original *T. th.* SG project, the differences in the used expression vectors, especially the presence of a polyhistidine tag and the protease recognition site in the pET-47md backbone, seem to have affected the solubility of the *T. th.* proteins.

Then we tested the expression level and the solubility of *T. th.* tag-fused Vpr. Except for tags Tth1, Tth8, and Tth11, all *T. th.* tags facilitate the expression level of the fusion protein when the *T. th.* proteins had been added at the N terminus of Vpr (Fig. 2C, tth–vpr). However, in the case of C terminus addition, only the Tth6-fused protein among the *T. th.* tag-fused Vpr proteins was expressed well (Fig. 2C, vpr–tth).We found that the Tth2 protein enhanced the solubility of Vpr when Tth2 was added to the N terminus of Vpr (Fig. 2C).

Efficacy of the tag proteins on other insoluble proteins

We investigated the efficacy of *T. th.* tag proteins on other insoluble proteins from primate lentiviruses. Based on the results of *T. th.* alone or *T. th.* in a Vpr fusion form (Fig. 2), seven *T. th.* tags (Tth2, Tth3, Tth6, Tth9, Tth10, Tth11, and Tth13) were introduced to the N terminus of two lentiviral proteins. Three conventional tags were also introduced to this position. One of these proteins, gp41-MSD, is a highly hydrophobic 2.2-kDa peptide that anchors the envelope protein to lipid bilayers [27]. The synthetic peptide of gp41-MSD remains insoluble under the condition of 100% dimethyl sulfoxide (unpublished data). Another protein, Vpx, is a virion-associated 12.9-kDa protein of SIV that plays an important role in nuclear transport of the incoming preintegration complex [26]. Vpr and Vpx are evolutionarily related to each other and have approximately 15% of their primary structures in common. Among the conventional tags, MBP and NusA enhanced the expression level of tag-fused gp41-MSD (Fig. 3A), but the expressed proteins could not be found in the soluble fractions (Fig. 3A). Six *T. th.* tags (Tth2, Tth6, Tth9, Tth10, Tth11, and Tth13) enhanced expression levels when fused at the N terminus (Fig. 3B). Both the Tth2 and Tth10 proteins were partially successful at solubilizing gp41-MSD (Fig. 3B). In the case of Vpx, expression levels were enhanced when fused with NusA, Tth2, Tth3, Tth6, Tth9, Tth10, Tth11, and Tth13, although none of these fusion proteins could be solubilized (data not shown). These results suggest that *T. th.*-tagged proteins can enhance the expression level of insoluble proteins; however, the efficacy depends heavily on the passenger proteins used.

Effect of tag proteins on the function of passenger proteins

It is of interest to know whether fusion of a tag may affect any functions of the fused passenger protein. We attempted to test what effect, if any, the *T. th.* tag-fused Vpr had on the cell cycle, but our efforts at transduction of the purified proteins into the mammalian cells were not too successful. In the case of gp41-MSD, there is no good biological assay because it is a portion of a protein. Therefore, we used GFP as a surrogate reporter for Tth2, Tth6, Tth9, Tth10, Tth11, and Tth13. Most of the tag proteins, such as Tth2, Tth3, Tth6, and Tth9, enhanced expression to levels comparable to those achieved with the conventional tags GST and NusA (Fig. 4A). Moreover, Tth2, Tth10, and Tth13 proteins enhanced the solubility of fused GFPs. The fluorescence-activated cell sorting (FACS) analyses of the fluorescence of the fused GFPs showed that the fluorescent intensity of MBP, GST, Tth11, and Tth13 fused proteins was less than half the intensity of intact GFP (Fig. 4B). As shown in Fig. 4A, both the expression level and solubility of these fusion proteins were similar to those of intact GFP; however, the fusion with these tags reduced the activity of GFP. In the case of Tth2, Tth3, Tth6, Tth9, and Tth10 proteins, the fusion affected the fluorescence of GFP only slightly.

We next examined the stability of the tagged GFPs under denaturing conditions by treating the proteins with GdmHCl (Fig. 4C and D). For the conventional tag proteins, the denaturation profile of GST-fused GFP was nearly identical to that of intact GFP, although for MBP and NusA the normalized fluorescence intensities of the tag-fused proteins were slightly lower than the intensity of intact GFP (Fig. 4C). On the other hand, all denaturation profiles of *T. th.* tag-fused proteins, except for Tth13, were similar to the profile of tag-free GFP (Fig. 4D). These results suggest that the *T. th.* tag proteins do not destabilize the GFP passenger protein. We also observed the endurance of the tag-fused proteins to heat treatment (see Supplemental Fig. 1 in supplementary material), suggesting the possibility of a simple purification protocol employing a heat treatment.

Purification and characterization of tag-fused proteins

To verify whether a large amount of tag protein can be obtained using a *T. th.* tag-mediated system, large-scale expression and purification were performed. Tth2- or Tth10-fused protein was used because these two tags could efficiently solubilize insoluble protein. After induction, the proteins were purified in two steps: using nickel–nitrilotriacetate (Ni–NTA) columns and through size exclusion (Fig. 5A). Despite the good expression, the Tth2–Vpr protein was harder to purify, probably owing to the residual insoluble properties derived from Vpr. Except for the Tth2–Vpr protein, at least 1 mg of pure protein was obtained from a 1-L culture. Meanwhile, because a high concentration of salt improved the solubility of tag-fused proteins, 0.5 M NaCl was added at all of the purification and analysis steps. CD spectra of purified proteins were measured. CD of the Tth2 protein showed the typical pattern of an α-helix-containing protein, which has negative maxima at 209 and 222 nm (Fig. 5B), consistent with the results of crystal structure of Tth2 protein (PDB ID: 1WF4). Other proteins fused with Tth2 proteins, such as Tth2–GFP, Tth2–Vpr, and Tth2–gp41-MSD, also

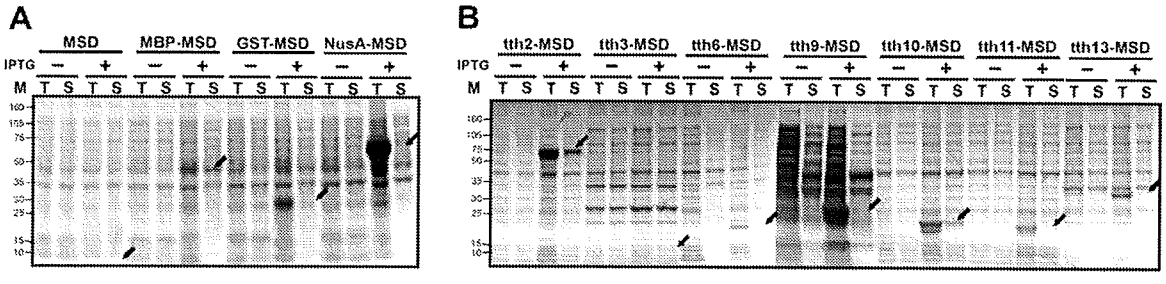

Fig. 3. Efficacy of tag protein for the expression of insoluble protein, gp41-MSD (MSD) from HIV-1. (A) Expression profiles of MSD alone and when fused with each of three conventional tags: MBP, GST, and NusA. (B) Expression profiles of tth-fused MSD. Each arrow indicates the position of the expected molecular weight of the fusion protein. Abbreviations are as defined in Fig. 2.